INTERNATIONAL JOURNAL FOR NUMERICAL METHODS IN ENGINEERING
Int. J. Numer. Meth. Engng (2010)
Published online in Wiley InterScience (www.interscience.wiley.com). DOI: 10.1002/nme.2849

On multiscale non-equilibrium molecular dynamics simulations

Shaofan Li[1,*,†] and Ni Sheng[2]

[1]*Department of Civil and Environmental Engineering, University of California, Berkeley, CA 94720, U.S.A.*
[2]*Faculty of Management and Administration, Macau University of Science and Technology, Macau S.A.R., People's Republic of China*

SUMMARY

In this work, we set forth a multiscale non-equilibrium molecular dynamics (MS-NEMD) model. The main objectives of MS-NEMD model are: (1) establishing a rigorous NEMD that provides direct three-dimensional simulations of thermal–mechanical motions at atomistic scale, and (2) providing a general computational paradigm for non-equilibrium multiscale simulations. The proposed MS-NEMD combines a coarse-grained continuum thermodynamics model with a fine scale NEMD simulation. A novel concept of *Multiscale Canonical Ensemble* is put forth, in which we argue that the coarse-grained field may provide a heat bath within the coarse scale relaxation time interval, while the fine scale motion may reach to a local equilibrium state during that time interval. In this work, we propose to use a Nosé–Hoover thermostat network that is distributed among the local Voronoi cell-ensembles, and it will then regulate the difference between the coarse scale thermodynamic temperature and kinetic temperature of the fine scale ensemble. The proposed MS-NEMD algorithm has the following features: (1) the fine scale distribution function is canonical in the sense that it obeys a drifted local Boltzmann distribution and (2) it can spontaneously and automatically return to the equilibrium state. Several numerical examples have been carried out, in which we have simulated the activation of shock waves or dislocations due to thermal fluctuations. Copyright © 2010 John Wiley & Sons, Ltd.

Received 19 May 2009; Revised 27 October 2009; Accepted 21 December 2009

KEY WORDS: dislocation; molecular dynamics; multiscale simulation; nanomechanics; non-equilibrium thermodynamics

1. INTRODUCTION

The non-equilibrium thermal–mechanical coupling process at small scales is a subject of increasing importance to energy conversion/transfer, biochemistry, cellular and molecular biology, micro- and nanoelectronics, and material synthesis and failure analysis. In principle, the essence of heat

*Correspondence to: Shaofan Li, Department of Civil and Environmental Engineering, University of California, Berkeley, CA 94720, U.S.A.
†E-mail: li@ce.berkeley.edu

Contract/grant sponsor: NSF; contract/grant number: CMMI-0800744

transfer at small scales is thermal–mechanical multiscale coupling, in which the length and time scales span from molecular level to continuum level. Both the subject as well as the definition of non-equilibrium thermodynamics have been studied before by many people, e.g. [1, 2]. Since that this work is a practical treatise of multiscale non-equilibrium molecular dynamics (MS-NEMD), in this work the non-equilibrium thermodynamic process is referred to as a process where both spatial and temporal gradients of the temperature field are non-trivial. In other words, the focus of the work is on NEMD, and it is beyond the finite temperature equilibrium molecular dynamics, which has been well studied in the past, e.g. [3].

A fundamental understanding of thermal–mechanical couplings in non-equilibrium states at small scales and the capacity to simulate such physical phenomena are vital to the study of the mechanism of energy transfer/conversion and the advancement of reliability of micro- and nanoelectronics. For example, understanding heat conduction in a nanotube or a nanowire is the key for such nanoscale structures being used in electronic devices and functioning properly under working conditions.

Since 1970s, NEMD method has been a major numerical tool for simulations of non-equilibrium thermal–mechanical coupling process. It has been extensively used in many scientific and engineering fields. Currently, several types of NEMDs are used in different research fields. Here, we briefly review some of the representative NEMD algorithms:

1. Boundary-heat-flux-driven NEMD simulations: In this type of NEMD simulations the molecular dynamics system is driven out of equilibrium by prescribed boundary heat flux or temperature distribution, i.e. prescribed hot or cold heat sources or heat sinks at the boundaries of the domain of interest. Such heat sources or sinks are either maintained by thermostat techniques or velocity scaling techniques (e.g. [4–10], among many others). A main feature of this type of NEMDs is that in the interior domain only conventional molecular dynamics, i.e. the micro-canonical ensemble MD, is used in simulations, hence they are often referred to as *direct NEMD* or *natural NEMD*. In the rest of paper, we refer the boundary-heat-flux-driven NEMD simulations as *the direct NEMD simulations* or *the conventional NEMD simulations*. The direct NEMD simulations have been extensively used in thermal fluid science and engineering and applied physics communities, and they have been used as the workhorse in performing direct atomistic or molecular simulations in many scientific and engineering fields, including nanoscale heat transfer [7, 11], polymer and amorphous materials [12, 13], gas transport in nanopores [14], Raman response of liquids [15], filtering and separation of mixtures [16], among many other applications.
2. Boundary-velocity-flow-driven NEMD simulations: The representatives of such NEMD algorithms are the classic DOLLS and SLLOD algorithms proposed by Hoover, Evans, and Morris [17–21]. The SLLOD algorithm is a symmetric version of DOLLS algorithm, and it has been extensively used for simulations of planar Couette flows. In SLLOD algorithm, the molecular system is driven out of equilibrium by mechanical boundary conditions. Most applications of SLLOD algorithm for modeling shear flow use the Lees–Edwards boundary conditions, and most applications of SLLOD algorithm for modeling elongational flow use the Kraynik–Reinelt boundary conditions. Recently a so-called proper SLLOD algorithm (p-SLLOD) has been proposed, and it is proven to be theoretically rigorous to simulate general inhomogeneous flows [22–26]. The boundary-velocity-flow-driven NEMD algorithms have been used in computing transport coefficients [27–29], simulating viscous flows [18, 20, 24] and plastic deformations [30, 31], among others. Although there were attempts to thermalize

DOI: 10.1002/nme

these algorithms, so that both mechanical and thermal boundary conditions can be applied at the same time, e.g. [21], most of these algorithms are just using Newton's equations of motions in the interior of the simulation domain to extract thermodynamics properties. In other words, if we consider that the boundary-thermostated region is just a means to prescribed heat flux, the direct NEMD is in fact a micro-canonical ensemble MD in the interior domain of the simulation domain, in which all the atoms are not thermostated, with the prescribed heat flux boundary condition at both ends. Till date, a NEMD that can couple thermal–mechanical interactions is yet to be established.

3. The synthetic NEMD simulations: In this type of NEMD simulations an artificial external field is globally prescribed to drive the system out of equilibrium [21, 28, 32–34]. In practice, the artificial external field is judicially chosen such that it renders the phase-space flux divergence-free, or it satisfies a so-called *adiabatic incompressibility condition* ($AI\Gamma$) [21]. In Evans and Morriss [21], various thermostats are discussed for such type of algorithms. Moreover, the synthetic NEMD simulations are linked with the Green–Kubo's linear response theory, and they have been used to extrapolate the transport coefficients of non-equilibrium states. In practice, this type of NEMD algorithms are formulated under special conditions for particular purposes, e.g. simulation of transport coefficients, and therefore in general they are not intended or have not been used as a direct simulation tool.

The above categorization of NEMD simulations may be oversimplified. The present work, however, only concerns with the direct NEMD simulations, which have been the workhorse in thermal–mechanical engineering simulations. We have found that the direct NEMD simulations are not able to automatically or spontaneously return to a canonical ensemble equilibrium state when the external disturbances disappear. The reason is that the direct NEMD simulations use the micro-canonical ensemble MD in the interior domain and impose the fixed temperature values only at the boundary. This can be demonstrated by an one-dimensional (1D) example shown in Figure 1, in which we compare a direct NEMD simulation with a Nośe–Hoover equilibrium MD simulation. The Nosé–Hoover equilibrium MD is a canonical ensemble MD under equilibrium state. In order to maintain a fixed temperature, the atomistic or molecular system is regularized by a Nośe–Hoover thermostat [3] or a Nośe–Hoover thermostat chain [35]. For simplicity, let the interatomic force be from the pair potential only. Then the Nosé–Hoover equilibrium MD simulation may take the following form [3, 6]:

$$m_i\ddot{q}_i = F(q_i - q_{i-1}) - F(q_{i+1} - q_i) - \xi_T m_i \dot{q}_i, \quad i = 1, 2, \ldots, N \tag{1}$$

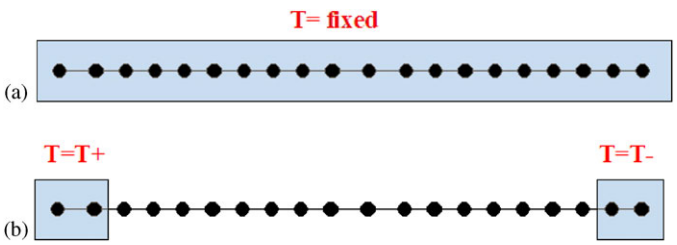

Figure 1. Comparison between (a) the Nośe–Hoover equilibrium MD simulation and (b) the direct NEMD simulation.

DOI: 10.1002/nme

where q_i is the position of atom i, m_i is its mass, F is the potential force, and ξ_T is an auxiliary variable that may be determined by the following equation:

$$\frac{\mathrm{d}\xi_T}{\mathrm{d}t}=\frac{1}{\Theta}\left(\sum_{j=1}^{N} m_j\dot{q}_j^2-k_{\mathrm{B}}NT\right) \tag{2}$$

where k_{B} is the Boltzmann constant, N is the total number of atoms, T is the equilibrium temperature, and Θ is the pseudo mass of ξ_T.

For the direct NEMD simulation, only the boundary regions Ω_+ and Ω_- are thermostated with the temperatures T_+ and T_-, respectively. If we use $S_\pm$ and $N_\pm$ to, respectively, denote index sets and numbers of atoms in boundary regions, the governing equations can be written as:

$$m_i\ddot{q}_i=F(q_i-q_{i-1})-F(q_{i+1}-q_i)-\begin{cases}\xi_+ m_i\dot{q}_i & \text{if } i\in S_+\\ \xi_- m_i\dot{q}_i & \text{if } i\in S_-\end{cases} \tag{3}$$

where

$$\frac{\mathrm{d}\xi_\pm}{\mathrm{d}t}=\frac{1}{\Theta_\pm}\left(\sum_{j=1}^{N_\pm} m_j\dot{q}_j^2-k_{\mathrm{B}}N_\pm T_\pm\right). \tag{4}$$

One can see clearly that Equations (3) and (4) will not degenerate to (1) and (2) even if we choose $T_+=T_-=T$ and make $\Theta_+=\Theta_-=\Theta$. The reason is that in the direct NEMD simulation, the interior domain is not thermostated and it is treated via classical micro-canonical ensemble MD simulation.

The micro-canonical ensemble MD simulation is deterministic in nature, and whether it can faithfully model the statistical phonon scattering process in the interior domain without ubiquitous presence of random forces is in question. For instance, Chen [36] expressed the same concern on statistical physics foundation of the direct NEMD simulation.

In most direct NEMD simulations, when the whole system reaches to a non-equilibrium steady state, the local equilibrium assumption is adopted to measure the local temperature. On the other hand, in the steady-state region, the micro-canonical ensemble MD is used in the NEMD simulation, the application of the equipartition theorem to obtain local temperature has been unjustifiably used in practice by assuming the presence of a local Boltzmann distribution function, which is in contradiction with the use of micro-canonical ensemble MD. Moreover, if a system's temperature is below the Debye temperature (see Table I, the quantum correction may be necessary e.g. [37, 38], the integration of the direct NEMD simulation with quantum correction has also been unjustifiably used, because the quantum correction may be only applicable to a classical canonical ensemble.

At the fundamental level, the local equilibrium assumption is related to or equivalent to an ergodic assumption, because we can only use the spatial average to replace the temporal average for a local canonical ensemble and the same may not be true for general non-equilibrium states.

Table I. Debye temperatures of various solids.

Silicon (Si)	Diamond	Titanium (Ti)	α-Iron	Aluminum (Al)	Copper (Cu)
640 K	2200 K	420 K	464 K	426 K	344.5 K

DOI: 10.1002/nme

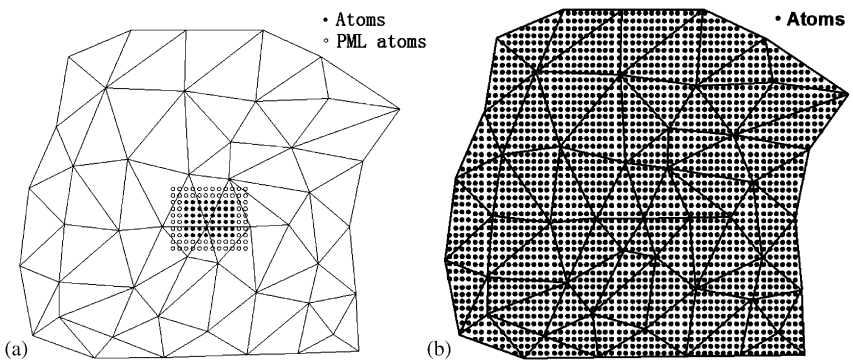

Figure 2. (a) The usual concurrent multiscale simulation and (b) the proposed multiscale NEMD simulation: fine scale region is marked with black dot and coarse scale region is represented by finite element discretization.

Because of its broad applications, it seems to us that it may be necessary to develop a NEMD simulation technique with solid statistical mechanics foundation for direct simulations of non-equilibrium systems that have both spatial and temporal temperature gradients.

Recently, a class of concurrent multiscale simulations have emerged in nanoscale computational mechanics, for example the heterogeneous multiscale method [39, 40], the bridging scale method [41–43], the finite temperature quasi-continuum method [44, 45], the bridging domain method [46], the perfectly matched multiscale simulation [47–49], and among others. The basic idea of the concurrent multiscale simulations is shown in Figure 2(a): a coarse scale model is applied to the entire domain of the problem interested; and a fine scale model is only used in a subregion where finer resolution is required, for example the places where thermal–mechanical fluctuation caused by inhomogeneities is so prevalent that it not only dictates the fine scale statistical thermodynamics, but also affects the coarse scale thermodynamics.

The concurrent multiscale simulations are suited to model physical phenomena operating across different scales and have become a popular research topic in recent years. However, most of the multiscale models in the literature focus either on solving problems at zero temperature or on simulating equilibrium systems with uniform environmental temperature. To the best of our knowledge, there are few multiscale simulations or formulations available for non-equilibrium systems, if there are any at all. In this paper, the term *non-equilibrium multiscale simulation* is referred to a concurrent multiscale paradigm that couples a thermal–mechanical simulation at continuum or quasi-continuum scale, e.g. heat transfer simulation with thermo-mechanical interactions, with a NEMD at atomistic scale. However, in general this definition can be extended to the concurrent multiscale coupling between Boltzmann transport equation and NEMD or the concurrent multiscale coupling between the electron transport simulation and a time-dependent density functional theory simulation.

In a recent letter [50], the present authors have proposed a canonical multiscale non-equilibrium method, which is the further development of the previous work [49]. This work is a comprehensive treatise of the proposed MS-NEMD. We would like to *point out* that the objective of the proposed MS-NEMD is fundamentally different from that of the usual concurrent multiscale simulation models: the present multiscale model is to use concurrent multiscale simulation techniques developing a NEMD algorithm with multiscale characters that can correctly represent non-equilibrium

DOI: 10.1002/nme

statistical physics and simulate non-equilibrium thermal–mechanical interactions at atomistic scale whereas the most previous concurrent multiscale simulations are aimed at saving computation cost for large-scale atomistic simulations. We would like to stress that the main difference between the present work and the previous concurrent multiscale models is that we are not concerned with developing a general multiscale algorithm to save Central Processing Unit (CPU) at the present stage but developing a physically correct NEMD model. For the proposed MS-NEMD algorithm, its computational cost may be even more expensive than that of the direct NEMD; however, it sets a foundation for a more general MS-NEMD model that can save computational resources significantly while providing physically correct predictions.

In this work, the coarse scale and the fine scale dynamics coexist in the same region, see Figure 2(b), and we are concerned with the multiscale coupling inside the region where the coarse scale and fine scale dynamics are present. The coarse scale and the fine scale are different layers of the same spatial region, and we do not have, hence do not discuss, any issues of the coupling of the atomistic simulation and the continuum simulation in different spatial regions. The meaning of the concurrent simulation refers to different but synchronized dynamics in different layers (scales). For this reason, the paper's title is multiscale non-equilibrium molecular dynamics rather than multiscale non-equilibrium simulation. In that case, we have to address the treatment of multiscale boundary conditions between the fine scale NEMD and the coarse scale heat transfer equation, similar as what have been discussed in [51, 52]. Nevertheless, this work may provide a foundation for a general multiscale non-equilibrium simulation theory that will be the future study of this research.

We term the proposed algorithm as the MS-NEMD algorithm, because we study the dynamics of the non-equilibrium system at both macroscale (or mesoscale) and microscale (atomistic scale) concurrently and simultaneously.

In the proposed MS-NEMD algorithm, the non-equilibrium thermodynamics of the mean drifting field, or the thermodynamics of the coarse-grained field, is concurrently computed by the finite element method with inputs from fluctuations of fine scale atomistic field besides the macroscale boundary and initial conditions; whereas in the fine scale the molecular dynamics simulation is driven by random forces that are regulated by macroscale heat transfer through a distributed Nośe–Hoover thermostat network.

The fine scale motion in each thermostat is assumed to reach to a local equilibrium state during the coarse scale relaxation time interval, and can be computed by the Nosé–Hoover equilibrium MD algorithm. The fine scale motion is driven out of the equilibrium by the coarse scale mean field instead of a prescribed or fictitious external field as in some traditional NEMD simulations. In return, the fine scale simulation results are used to update temperature and displacement fields at the coarse-grained level, and they may also be used to calculate transport coefficients for the coarse-grained formulation. It is shown that under the local equilibrium assumption the proposed MS-NEMD algorithm may produce a canonical NEMD simulation.

This paper is organized as follows: in Section 2, we first introduce the multiscale decomposition used in the proposed multiscale formulation, which is crucial to the construction of a canonical NEMD simulation. In Section 3, we elaborate the MS-NEMD algorithm both from theoretical foundation and in algorithmic details. Then we shall further prove that the fine scale distribution function is canonical. We shall discuss the coarse scale thermodynamics formulation in Section 4. The implementation of the MS-NEMD algorithm is described in Section 5. Three numerical examples are presented in Section 6, which include the simulations of thermal activation of shock waves. Finally, we conclude the presentation in Section 7 by making a few remarks.

DOI: 10.1002/nme

2. MULTISCALE DECOMPOSITION AND CENTER OF MASS FRAME

An important step in NEMD calculation is the use of the peculiar and the associated center of mass (COM) coordinates, with which one can rigorously extract thermodynamics properties of the system from the drifting frame of reference [21, 53]. In fact, thermodynamic properties of a non-equilibrium system like temperature are defined in terms of peculiar velocity field. If a finite continuum thermodynamic system is undergoing large deformation under non-equilibrium conditions, it may not be sufficient to use only one set of COM coordinates. For each statistical ensemble element, one needs a set of local peculiar and COM coordinates to define the local peculiar velocities.

By using a multiscale decomposition, we generalize the concepts of the peculiar and COM coordinates to establish the coarse scale field corresponding to the generalized COM coordinates and the fine scale field corresponding to the generalized peculiar coordinates. Hence, the multiscale decomposition is the foundation of the concurrent MS-NEMD algorithm.

We view the multiscale decomposition proposed in [41] as an extension of the peculiar and COM coordinates, which decomposes the discrete atomistic displacement field, $\mathfrak{q}$, into a coarse scale part and a fine scale part:

$$\mathfrak{q} = \bar{\mathfrak{q}} + \mathfrak{q}' \tag{5}$$

The symbol $\bar{}$ indicates coarse scale quantities, the symbol $'$ denotes their fine scale counterparts, and the matrix notation is implied in (5)

$$\mathfrak{q} = [\mathbf{q}_1, \ldots, \mathbf{q}_i, \ldots, \mathbf{q}_{n_{\text{atom}}}]^{\text{T}} \tag{6}$$

where $\mathbf{q}_i = q_{i1}\mathbf{E}_1 + q_{i2}\mathbf{E}_2 + q_{i3}\mathbf{E}_3$ is the total displacement vector of the i-th atom, $\mathbf{E}_i, i = 1, 2, 3$ are the basis vectors of Cartesian coordinates in reference configuration, and n_{atom} is the total number of atoms in the system.

We assume that the coarse scale atomistic displacement field $\bar{\mathfrak{q}}$ can be described by a continuous displacement field,

$$\bar{\mathbf{u}}(\mathbf{X}) = \bar{u}_1(\mathbf{X})\mathbf{E}_1 + \bar{u}_2(\mathbf{X})\mathbf{E}_2 + \bar{u}_3(\mathbf{X})\mathbf{E}_3 \tag{7}$$

where $\mathbf{X}$ denotes the spatial position vector. In this paper, the continuous displacement field $\bar{\mathbf{u}}(\mathbf{X})$ is governed by a coarse-grained model that is constructed by incorporating with finite element (FE) method, so that the continuous displacement field can be interpolated by FE shape functions,

$$\bar{\mathbf{u}}(\mathbf{X}) = \sum_{I=1}^{n_{\text{node}}} N_I(\mathbf{X})\mathbf{d}_I \tag{8}$$

where

$$\mathbf{d}_I := d_{I1}\mathbf{E}_1 + d_{I2}\mathbf{E}_2 + d_{I3}\mathbf{E}_3 \tag{9}$$

is the displacement vector of the FE node I, n_{node} is the total number of FE nodes, and $N_I(\mathbf{X})$ is the conventional FE shape function associated with node I evaluated at $\mathbf{X}$ (e.g. see [54]). At atom sites, the continuous displacement field captures the coarse scale atomistic displacement field, i.e.

$$\bar{\mathbf{u}}(\mathbf{X}_i) = \sum_{I=1}^{n_{\text{node}}} N_I^i \mathbf{d}_I \tag{10}$$

DOI: 10.1002/nme

where $N_I^i := N_I(\mathbf{X}_i)$, and $\mathbf{X}_i$ is the spatial position vector of the i-th atom in the system.

Define the FE nodal displacement array as

$$\mathbb{d} = [\mathbf{d}_1, \ldots, \mathbf{d}_I, \ldots, \mathbf{d}_{n_{\text{node}}}]^{\text{T}} \tag{11}$$

and the FE shape function matrix $\mathbb{N}$ as

$$\mathbb{N} = \begin{bmatrix} N_1^1 \mathbb{I}^{3\times3} & N_2^1 \mathbb{I}^{3\times3} & \ldots & N_{n_{\text{node}}}^1 \mathbb{I}^{3\times3} \\ N_1^2 \mathbb{I}^{3\times3} & N_2^2 \mathbb{I}^{3\times3} & \ldots & N_{n_{\text{node}}}^2 \mathbb{I}^{3\times3} \\ \vdots & \vdots & \ddots & \vdots \\ N_1^{n_{\text{atom}}} \mathbb{I}^{3\times3} & N_2^{n_{\text{atom}}} \mathbb{I}^{3\times3} & \ldots & N_{n_{\text{node}}}^{n_{\text{atom}}} \mathbb{I}^{3\times3} \end{bmatrix} \tag{12}$$

where

$$\mathbb{I}^{3\times3} = [\delta_{ij}]^{3\times3}$$

is the 3×3 identity matrix and $\mathbb{N}$ is of size $3n_{\text{atom}} \times 3n_{\text{node}}$. The coarse scale atomistic displacement array can be expressed as

$$\bar{\mathbb{q}} = \mathbb{N}\, \mathbb{d} \tag{13}$$

where

$$\bar{\mathbf{q}} = [\bar{\mathbf{u}}(\mathbf{X}_1), \ldots, \bar{\mathbf{u}}(\mathbf{X}_i), \ldots, \bar{\mathbf{u}}(\mathbf{X}_{n_{\text{atom}}})]^{\text{T}} \tag{14}$$

Similarly, the total atomistic velocity array, $\dot{\mathbf{q}}$, can be decomposed into two scales,

$$\dot{\mathbb{q}} = \dot{\bar{\mathbb{q}}} + \dot{\mathbb{q}}' \tag{15}$$

in which the coarse scale atomistic velocity array can be expressed by FE interpolation,

$$\dot{\bar{\mathbb{q}}} = \mathbb{N}\, \dot{\mathbb{d}} \tag{16}$$

where $\dot{\mathbb{d}}$ is the FE nodal velocity array.

Define the atomistic mass matrix as

$$\mathbb{M}_A = \begin{bmatrix} m_1 \mathbb{I}^{3\times3} & & & \\ & m_2 \mathbb{I}^{3\times3} & & \\ & & \ddots & \\ & & & m_{n_{\text{atom}}} \mathbb{I}^{3\times3} \end{bmatrix} \tag{17}$$

the total linear momentum array of the atomistic system can be written as

$$\mathbb{p} = \mathbb{M}_A\, \dot{\mathbb{q}} \tag{18}$$

which can also be decomposed into two scales

$$\mathbb{p} = \bar{\mathbb{p}} + \mathbb{p}' \tag{19}$$

DOI: 10.1002/nme

To link the total displacement field $\mathbf{q}$ with the coarse scale displacement field $\bar{\mathbf{q}}$, Wagner and Liu [41] used the following weighted ℓ_2 type of error norm to minimize the difference between the total displacements and the coarse scale displacements at all atom positions, i.e.

$$\min_{\mathbf{d}} \sum_{i=1}^{n_{\text{atom}}} m_i \left| \mathbf{q}_i - \sum_{I}^{n_{\text{node}}} N_I^i \mathbf{d}_I \right|^2 \tag{20}$$

By doing so, both the coarse scale displacement field and the fine scale displacement field can be obtained from the total displacement field by the following projection operations,

$$\bar{\mathbf{q}} = \mathbb{P}\,\mathbf{q}, \quad \mathbf{q}' = \mathbb{Q}\,\mathbf{q} \tag{21}$$

where $\mathbb{P}$ and $\mathbb{Q}$ are projection matrices defined as

$$\mathbb{P} := [P_{ij}]^{3n_{\text{atom}} \times 3n_{\text{atom}}} = \mathbb{N}\mathbb{M}^{-1}\mathbb{N}^{\mathrm{T}}\mathbb{M}_A \tag{22}$$

$$\mathbb{Q} := [Q_{ij}]^{3n_{\text{atom}} \times 3n_{\text{atom}}} = \mathbb{I} - \mathbb{P} \tag{23}$$

where

$$\mathbb{I} = [\delta_{ij}]^{3n_{\text{atom}} \times 3n_{\text{atom}}}$$

is the $3n_{\text{atom}} \times 3n_{\text{atom}}$ identity matrix, and the matrix $\mathbb{M}$ is the coarse scale mass matrix defined as

$$\mathbb{M} := [M_{ij}]^{3n_{\text{node}} \times 3n_{\text{node}}} = \mathbb{N}^{\mathrm{T}}\mathbb{M}_A\mathbb{N} \tag{24}$$

It is readily verified that indeed the operators $\mathbb{P}$ and $\mathbb{Q}$ are projection operators, i.e.

$$\mathbb{P}\mathbb{P} = \mathbb{P} \quad \text{and} \quad \mathbb{Q}\mathbb{Q} = \mathbb{Q} \tag{25}$$

In [48], the present authors explored the physical meaning of the above multiscale decomposition. It is argued that the above projection operators can also be obtained by the following minimization procedure,

$$\min_{\dot{\mathbf{d}}} \left\{ \tfrac{1}{2} (\dot{\mathbf{p}}')^{\mathrm{T}} \mathbb{M}_A^{-1} \dot{\mathbf{p}}' \right\} = \min_{\dot{\mathbf{d}}} \left\{ \tfrac{1}{2} (\dot{\mathbf{q}} - \mathbb{N}\dot{\mathbf{d}})^{\mathrm{T}} \mathbb{M}_A (\dot{\mathbf{q}} - \mathbb{N}\dot{\mathbf{d}}) \right\} \tag{26}$$

for a fixed velocity field $\dot{\mathbf{q}}$. The minimization is attainable because $\mathbb{M}_A$ is positive definite. If we consider the fine scale velocity as the generalization of '*peculiar velocity field*' [21], the kinetic temperature may be defined by

$$\tfrac{3}{2}(n_{\text{atom}} - n_{\text{node}}) k_{\text{B}} T = \left\langle \tfrac{1}{2} (\dot{\mathbf{p}}')^{\mathrm{T}} \mathbb{M}_A^{-1} \dot{\mathbf{p}}' \right\rangle \tag{27}$$

where $\langle \cdot \rangle$ denotes averaging in time. Note that the definition of temperature in (27) has been adopted by both Wagner and Liu [41] and Rudd and Broughton [55]. We may argue that the physical implication of such multiscale decomposition is: '*For a system with given total kinetic energy and a priori coarse-grained dimension* (*size of the ensemble cell or FEM mesh*), *the multiscale projection operators are obtained based on the condition that among all possible coarse scale velocity fields* (*with the fixed degrees of freedom* n_{node}), *the projected coarse scale velocity field should describe the movement of the drifted center of mass manifold* (*mean field*) *upon which the temperature of the system can be corrected defined. In other words, the projected coarse scale*

DOI: 10.1002/nme

velocity field separates the fluctuation of the system from the total velocity field.' Therefore, we may call the decomposition or the projection as *the adiabatic decomposition or the adiabatic projection*, meaning that the decomposition itself will not cause thermal exchange between two scales. More precisely speaking, here the adjective 'adiabatic' means that the separation of the drifting coarse scale velocity field from the total velocity field will not cause any thermal energy leaking. This is the basis for establishing a COM continuum frame of coarse scale. Nevertheless, there are thermal exchanges between the coarse scale and the fine scale, and this is accomplished by using the coarse scale FEM nodal temperatures to enforce the local equilibrium temperature for each and every Nosé–Hoover thermostats.

A direct consequence of such decomposition is that it decouples the fine scale (or peculiar) velocity field with the coarse scale (or mean) velocity field. Considering the following coarse scale linear momentum field and the fine scale linear momentum field projected from the total linear momentum field,

$$\bar{\mathbb{p}} = \mathbb{P}\,\mathbb{p} \quad \text{and} \quad \mathbb{p}' = \mathbb{Q}\,\mathbb{p} \tag{28}$$

one can show that

$$(\mathbb{p}')^{\mathrm{T}}\mathbb{M}_A^{-1}\,\bar{\mathbb{p}} = \mathbb{p}^{\mathrm{T}}\mathbb{Q}^{\mathrm{T}}\mathbb{M}_A^{-1}\mathbb{P}\,\mathbb{p} = 0 \tag{29}$$

because of the identity $\mathbb{Q}^{\mathrm{T}}\mathbb{M}_A^{-1}\mathbb{P} \equiv 0$. Similarly,

$$\bar{\mathbb{p}}^{\mathrm{T}}\mathbb{M}_A^{-1}\,\mathbb{p}' = \mathbb{p}^{\mathrm{T}}\mathbb{P}^{\mathrm{T}}\mathbb{M}_A^{-1}\mathbb{Q}\,\mathbb{p} = 0 \tag{30}$$

For mono-atom systems, under multiscale projections (28), Equations (29) and (30) imply that the peculiar linear momentum field is orthogonal to the mean linear momentum field, i.e.

$$\sum_{i=1}^{n_{\mathrm{atom}}} \frac{1}{m_i}\mathbf{p}_i' \cdot \bar{\mathbf{p}}_i \equiv 0. \tag{31}$$

This orthogonal condition is crucial to the construction of the present multiscale NEMD algorithm, which will be discussed in the following section.

3. MULTISCALE NON-EQUILIBRIUM MOLECULAR DYNAMICS MODEL

The essence of the proposed MS-NEMD algorithm is: the coarse scale motion is solved by using the FE method based on a coarse-grained thermodynamics model, which is driven by macroscale initial/boundary conditions and the thermal fluctuation from the fine scale computation; whereas the fine scale motion is modeled and solved by using a NEMD simulation, which receives the inputs from the coarse scale computation and is driven out of the equilibrium by the coarse scale mean field instead of a prescribed or fictitious external field as in some traditional NEMD simulations, such as DOLLS or SLLOD algorithms.

A conceptual illustration of the multiscale framework is shown in Figure 3. In the proposed MS-NEMD model, we argue that a coarse scale FE node may be viewed as a '*coarse scale thermal reservoir*', and it represents the ambient space of a large set of atoms. We call each set of atoms surrounding a FE node as a Voronoi cell-ensemble. Note that the Voronoi cell or Voronoi tessellation is a dual structure of Delaunay triangulation [56], hence the cell structure is related to FE mesh or discretization.

DOI: 10.1002/nme

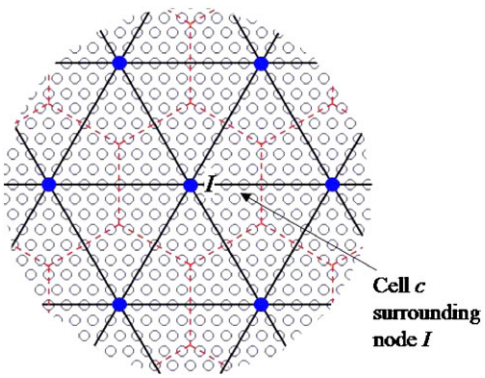

Figure 3. Coarse-grained FE mesh and Voronoi cell-ensemble structure.

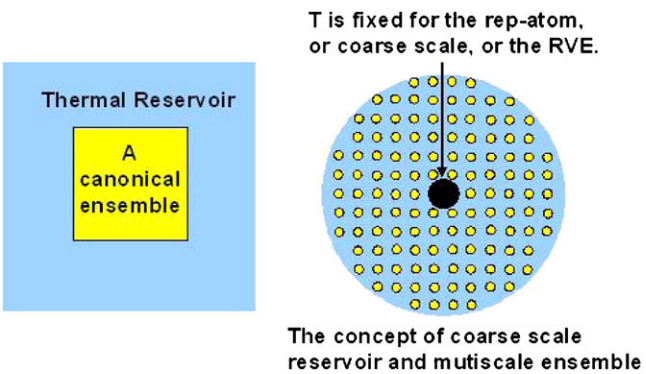

Figure 4. The illustration and comparison of canonical ensemble and multiscale canonical ensemble.

The main novelty of this work is the proposal of the concept, *multiscale canonical ensemble*, which is a generalization of the classical notion of canonical ensemble. The classical canonical ensemble, or fixed atom Number, Volume, and Temperature (NVT) ensemble, denotes a system embedded into an infinitely large thermal reservoir, whose temperature remains constant during an equilibrium process. In our model, we argue that the temperature of each coarse scale nodal reservoir remains constant during any time interval that is smaller than the time scale of the coarse grain, which is chosen here as the coarse scale time step. This claim is valid because the coarse grain is defined based on the '*slow variable approximation*' and the '*Markovian approximation*' [57]. Since a Voronoi cell-ensemble is embedded within a coarse scale nodal reservoir and the temperature of each coarse scale nodal reservoir remains constant within each coarse scale time step, the motions of atoms in a Voronoi cell-ensemble can be assumed to reach to a local equilibrium state within one coarse scale time step. So we may call a Voronoi cell-ensemble as a *multiscale canonical ensemble* in the sense of local equilibrium approximation, see Figure 4. The local equilibrium assumption has been widely used in non-equilibrium thermodynamics [21]. This work may be the first attempt to use it in multiscale analysis.

DOI: 10.1002/nme

In this section, we first discuss the fine scale NEMD algorithm. We consider the multiscale adiabatic Hamiltonian for a single cell-ensemble c surrounding the FE node I:

$$H_c^{\text{adia}} = \sum_{i=1}^{n_c} \frac{1}{2m_i}(\bar{\mathbf{p}}_i + \mathbf{p}'_i)\cdot(\bar{\mathbf{p}}_i + \mathbf{p}'_i) + U_c(\mathfrak{q})$$

$$= \sum_{i=1}^{n_c} \frac{1}{2m_i}\bar{\mathbf{p}}_i \cdot \bar{\mathbf{p}}_i + \sum_{i=1}^{n_c} \frac{1}{2m_i}\mathbf{p}'_i \cdot \mathbf{p}'_i + \sum_{i=1}^{n_c} \frac{1}{2m_i}\bar{\mathbf{p}}_i \cdot \mathbf{p}'_i + U_c(\mathbf{q}) \tag{32}$$

where n_c is the number of atoms in the cell-ensemble c, $U_c(\mathbf{q})$ is the atomistic potential, $\bar{\mathbf{p}}_i$ and $\mathbf{p}'_i$ are, respectively, the coarse scale and fine scale linear momentum vectors of the i-th atom. Note that each cell-ensemble has only one node, so the numberings I and c have one-to-one correspondence (see Figure 3).

With the multiscale decomposition introduced in Section 2, the fine scale linear momentum field is orthogonal to the coarse scale linear momentum field, see Equation (31). Therefore, Equation (32) can be written as:

$$H_c^{\text{adia}} = \sum_{i=1}^{n_c} \frac{1}{2m_i}\bar{\mathbf{p}}_i \cdot \bar{\mathbf{p}}_i + \sum_{i=1}^{n_c} \frac{1}{2m_i}\mathbf{p}'_i \cdot \mathbf{p}'_i + U_c(\mathfrak{q}) \tag{33}$$

The two-scale equations of motion are then derived from Equation (33) as

$$\dot{\mathbf{q}}_i = \frac{\partial H_c^{\text{adia}}}{\partial \mathbf{p}_i} = \frac{\bar{\mathbf{p}}_i}{m_i} + \frac{\mathbf{p}'_i}{m_i} \tag{34}$$

$$\dot{\mathbf{p}}_i = -\frac{\partial H_c^{\text{adia}}}{\partial \mathbf{q}_i} = -\frac{\partial U(\mathfrak{q})}{\partial \mathbf{q}_i} =: \mathbf{F}_i \tag{35}$$

$$\dot{\bar{\mathbf{q}}}_i = \frac{\partial H_c^{\text{adia}}}{\partial \bar{\mathbf{p}}_i} = \frac{\bar{\mathbf{p}}_i}{m_i} \tag{36}$$

$$\dot{\bar{\mathbf{p}}}_i = -\frac{\partial H_c^{\text{adia}}}{\partial \bar{\mathbf{q}}_i} = \mathbf{F}_j \cdot \frac{\partial \mathbf{q}_j}{\partial \bar{\mathbf{q}}_i} \tag{37}$$

where $\mathbf{F}_i$ is the external force acting on the atom i. From Equations (34)–(35), the fine scale equations of motion may be expressed in terms of $\mathbf{q}_i$ and $\mathbf{p}'_i$ as follows:

$$\dot{\mathbf{q}}_i = \frac{\bar{\mathbf{p}}_i}{m_i} + \frac{\mathbf{p}'_i}{m_i} \tag{38}$$

$$\dot{\mathbf{p}}'_i = \mathbf{F}_i - \dot{\bar{\mathbf{p}}}_i \tag{39}$$

In passing we note that if the use of FE interpolation over the current configuration were justifiable, for instance the updated Lagrangian FE formulation was used [58], one might find that

$$\dot{\bar{\mathbf{p}}}_i = m_i \frac{\mathrm{d}}{\mathrm{d}t}(\dot{\bar{\mathbf{q}}}_i) = m_i \frac{\mathrm{d}}{\mathrm{d}t}\left(\sum_I N_I(\mathbf{x}_i)\dot{\mathbf{d}}_I\right)$$

$$= m_i\left(\sum_I N_I(\mathbf{x}_i)\ddot{\mathbf{d}}_I + \sum_I B_I(\mathbf{x}_i)\cdot\dot{\mathbf{x}}_i\dot{\mathbf{d}}_I\right) \tag{40}$$

DOI: 10.1002/nme

where

$$B_I(\mathbf{x}_i) := \frac{\mathrm{d}N_I(\mathbf{x}_i)}{\mathrm{d}\mathbf{x}_i}$$

and $\mathbf{x}_i$ is the current atom position denoted as $\mathbf{x}_i = \mathbf{q}_i + \mathbf{X}_i$. Thus, we have

$$\dot{\mathbf{x}}_i = \dot{\mathbf{q}}_i = \dot{\bar{\mathbf{q}}}_i + \frac{\mathbf{p}_i^{'}}{m_i} \tag{41}$$

which leads to

$$\begin{aligned}
\dot{\bar{\mathbf{p}}}_i &= m_i \left\{ \sum_I N_I(\mathbf{x}_i)\ddot{\mathbf{d}}_I + \sum_I (B_I(\mathbf{x}_i)\cdot\dot{\bar{\mathbf{q}}}_i)\dot{\mathbf{d}}_I + \sum_I \left(B_I(\mathbf{x}_i)\cdot\frac{\mathbf{p}_i'}{m_i}\right)\dot{\mathbf{d}}_I \right\} \\
&= m_i \frac{\mathrm{d}}{\mathrm{d}t}\left(\sum_I N_I(\mathbf{x}_i)\dot{\mathbf{d}}_I \right)_{\text{coarse scale}} + \sum_I (B_I(\mathbf{x}_i)\cdot\mathbf{p}_i')\dot{\mathbf{d}}_I \\
&\approx \sum_I (B_I(\mathbf{x}_i)\dot{\mathbf{d}}_I)\cdot\mathbf{p}_i' = \frac{\partial\dot{\bar{\mathbf{q}}}_i}{\partial\mathbf{x}_i}\cdot\mathbf{p}_i'
\end{aligned} \tag{42}$$

where we assume that

$$\begin{aligned}
m_i \frac{\mathrm{d}}{\mathrm{d}t}\left(\sum_I N_I(\mathbf{x}_i)\dot{\mathbf{d}}_I \right)_{\text{coarse scale}} &= m_i \left\{ \sum_I N_I(\mathbf{x}_i)\ddot{\mathbf{d}}_I + \sum_I (B_I(\mathbf{x}_i)\cdot\dot{\bar{\mathbf{q}}}_i)\dot{\mathbf{d}}_I \right\} \\
&\approx 0
\end{aligned} \tag{43}$$

when there is no external force at coarse scale. In this hypothetical case the MS-NEMD algorithm degenerates to a generalized mean-field driven DOLLS formulation. Nevertheless in the present paper, we have not pursued such formulation, and all the derivations here are based on the total Lagrangian formulation.

To couple the fine scale motions of atoms with the coarse scale heat conduction, we introduce a local Nosé–Hoover thermostat in each cell-ensemble such that the fine scale equations of motion in Equations (38) and (39) become

$$\dot{\mathbf{q}}_i = \frac{\mathbf{p}_i'}{m_i} + \frac{\bar{\mathbf{p}}_i}{m_i} \tag{44}$$

$$\dot{\mathbf{p}'}_i = \mathbf{F}_i - \dot{\bar{\mathbf{p}}}_i - \xi_c \mathbf{p'}_i \tag{45}$$

$\forall i \in \mathbf{n}_c$, $\mathbf{n}_c = \{1, \cdots\cdots, n_c\}$ and

$$\dot{\xi}_c = \frac{1}{\Theta_c}\left(\sum_{i\in\mathbf{n}_c} \frac{\mathbf{p'}_i\cdot\mathbf{p'}_i}{m_i} - 3n_c k_{\mathrm{B}} T_c \right) \tag{46}$$

where ξ_c is an auxiliary variable, Θ_c is the pseudo mass of ξ_c, and the temperature T_c for each cell-ensemble is the coarse scale thermodynamic temperature at FE node I. Equation (46) is another novelty of the present multiscale formulation. Since the coarse scale temperature distribution is not uniform and evolving with time, the FE nodal temperature changes from node to node and

DOI: 10.1002/nme

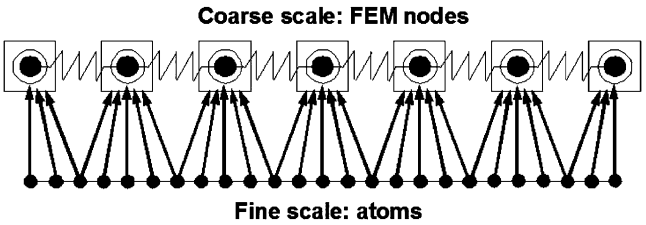

Figure 5. Distributed Nosé–Hoover thermostat network.

time to time. Therefore, the local thermodynamic temperature is not uniform among different cell-ensembles and different coarse scale time steps. In the MS-NEMD simulation, *a distributed Nosé–Hoover thermostat network* is used to ensure each cell-ensemble reaching to a local equilibrium state (see Figure 5). This is a generalization of the Nosé–Hoover thermostat [3, 35, 59, 60] in a global equilibrium ensemble MD simulation. In each cell-ensemble, the current environment temperature is set as thermodynamic temperature at the coarse scale FE node of previous time step. As discussed in [61], the damping term in molecular dynamics due to the Nosé–Hoover thermostat is in fact equivalent to a random force term. In this sense, one may view the distributed Nosé–Hoover thermostat network as a means to control the magnitude and the distribution of random forces applying to the fine scale atomic motions.

The conventional Nosé–Hoover thermostat renders the molecular dynamics system a canonical ensemble [59]. Will the proposed Nosé–Hoover thermostat network play a similar role in non-equilibrium simulations? Consider

$$H_c^* = \sum_{i=1}^{n_c} \frac{\bar{\mathbf{p}}_i \cdot \bar{\mathbf{p}}_i}{2m_i} + \sum_{i=1}^{n_c} \frac{\mathbf{p}'_i \cdot \mathbf{p}'_i}{2m_i} + U_c(\mathbf{q}) + J_{c+1} - J_{c-1} \tag{47}$$

where J_{c+1} and J_{c-1} are cell boundary fluxes. It then can be shown that

$$\begin{aligned} \frac{\mathrm{d}}{\mathrm{d}t} H_c^* - \dot{J}_{c+1} + \dot{J}_{c-1} &= \sum_i \left(\frac{1}{m_i} (\dot{\mathbf{p}}'_i \cdot \mathbf{p}'_i + \dot{\bar{\mathbf{p}}}_i \cdot \bar{\mathbf{p}}_i) - \mathbf{F}_i \cdot \dot{\mathbf{q}}_i \right) \\ &= \sum_i \left(\frac{1}{m_i} (\dot{\mathbf{p}}'_i \cdot \mathbf{p}'_i + \dot{\bar{\mathbf{p}}}_i \cdot \bar{\mathbf{p}}_i) - \mathbf{F}_i \cdot \left(\frac{\mathbf{p}'_i}{m_i} + \frac{\bar{\mathbf{p}}_i}{m_i} \right) \right) \\ &= \sum_i \left(\frac{\bar{\mathbf{p}}_i}{m_i} \cdot (\dot{\bar{\mathbf{p}}}_i - \mathbf{F}_i) + \frac{\mathbf{p}'_i}{m_i} \cdot (\dot{\mathbf{p}}'_i - \mathbf{F}_i) \right) \end{aligned} \tag{48}$$

From Equation (45), we have

$$\dot{\bar{\mathbf{p}}}_i - \mathbf{F}_i = -\dot{\mathbf{p}}'_i - \xi_c \mathbf{p}'_i \tag{49}$$

$$\dot{\mathbf{p}}'_i - \mathbf{F}_i = -\dot{\bar{\mathbf{p}}}_i - \xi_c \mathbf{p}'_i \tag{50}$$

DOI: 10.1002/nme

which lead to:

$$\begin{aligned}\frac{\mathrm{d}}{\mathrm{d}t}H_c^* - \dot{J}_{c+1} + \dot{J}_{c-1} &= \sum_i \left(\frac{\bar{\mathbf{p}}_i}{m_i}(-\dot{\mathbf{p}}'_i - \xi_c \mathbf{p}'_i) + \frac{\mathbf{p}'_i}{m_i}(-\dot{\bar{\mathbf{p}}}_i - \xi_c \mathbf{p}'_i) \right) \\ &= -\xi_c \left(\sum_i \frac{1}{m_i} \mathbf{p}'_i \cdot \mathbf{p}'_i \right) - \xi_c \left(\sum_i \frac{1}{m_i} \mathbf{p}'_i \cdot \bar{\mathbf{p}}_i \right) - \sum_i \left(\frac{1}{m_i}(\mathbf{p}'_i \cdot \dot{\bar{\mathbf{p}}}_i + \bar{\mathbf{p}}_i \cdot \dot{\mathbf{p}}'_i) \right) \\ &= -\xi_c \left(\sum_i \frac{1}{m_i} \mathbf{p}'_i \cdot \mathbf{p}'_i \right) - \xi_c \left(\sum_i \frac{1}{m_i} \mathbf{p}'_i \cdot \bar{\mathbf{p}}_i \right) - \frac{\mathrm{d}}{\mathrm{d}t} \left(\sum_i \frac{1}{m_i} \mathbf{p}'_i \cdot \bar{\mathbf{p}}_i \right) \end{aligned} \tag{51}$$

With the orthogonal condition in Equation (31), Equation (51) can be written as:

$$\frac{\mathrm{d}}{\mathrm{d}t}H_c^* = -\xi_c \left(\sum_i \frac{1}{m_i} \mathbf{p}'_i \cdot \mathbf{p}'_i \right) + \dot{J}_{c+1} - \dot{J}_{c-1}. \tag{52}$$

Now we consider the rate of change of the following pseudo-energy,

$$\frac{\mathrm{d}}{\mathrm{d}t} \left(H_c^* + \frac{1}{2}\Theta_c \xi_c^2 \right) = -\xi_c \left(\sum_i \frac{1}{m_i} \mathbf{p}'_i \cdot \mathbf{p}'_i \right) + \dot{J}_{c+1} - \dot{J}_{c-1} + \Theta_c \xi_c \dot{\xi}_c \tag{53}$$

By substituting Equation (46) into the above equation, we get

$$\frac{\mathrm{d}}{\mathrm{d}t} \left(H_c^* + \frac{1}{2}\Theta_c \xi_c^2 \right) = -3n_c \xi_c k_\mathrm{B} T_c + \dot{J}_{c+1} - \dot{J}_{c-1} \tag{54}$$

It should be pointed out that the Voronoi cell-ensemble is not isolated to each other. They are open systems with fluxes exchange from each other. Assume that the domain boundary is adiabatic, then the inter-cell fluxes cancel each other if we sum Equation (54) for all cell-ensembles. Thus,

$$\sum_c \left(\frac{\mathrm{d}}{\mathrm{d}t} \left(H_c^* + \frac{1}{2}\Theta_c \xi_c^2 \right) \right) = -\sum_c 3n_c \xi_c k_\mathrm{B} T_c. \tag{55}$$

On the other hand, the Liouville equation for distribution function is

$$\sum_c \frac{\mathrm{d}f_c}{\mathrm{d}t} = -\sum_c \left\{ f_c \sum_{i=1}^{n_c} \left(\frac{\partial \dot{\mathbf{q}}_i}{\partial \mathbf{q}_i} + \frac{\partial \dot{\mathbf{p}}'_i}{\partial \mathbf{p}'_i} \right) + f_c \frac{\partial \dot{\xi}_c}{\partial \xi_c} \right\} \tag{56}$$

where f_c is the probability density distribution function for cell-ensemble c. From Equation (44), we have

$$\frac{\partial \dot{\mathbf{q}}_i}{\partial \mathbf{q}_i} = \frac{\partial}{\partial \mathbf{q}_i} \left(\frac{\mathbf{p}'_i}{m_i} + \frac{\bar{\mathbf{p}}_i}{m_i} \right) = \frac{\partial \dot{\bar{\mathbf{q}}}_i}{\partial \mathbf{q}_i}. \tag{57}$$

From Equation (45), we have

$$\frac{\partial \dot{\mathbf{p}}'_i}{\partial \mathbf{p}'_i} = \frac{\partial}{\partial \mathbf{p}'_i}(\mathbf{F}_i - \dot{\bar{\mathbf{p}}}_i - \xi_c \mathbf{p}'_i) = -\frac{\partial \dot{\bar{\mathbf{p}}}_i}{\partial \mathbf{p}'_i} - 3\xi_c \tag{58}$$

By virtue of Equation (42),

$$\frac{\partial \dot{\bar{\mathbf{p}}}_i}{\partial \mathbf{p}'_i} = \frac{\partial \dot{\bar{\mathbf{q}}}_i}{\partial \mathbf{x}_i} = \frac{\partial \dot{\bar{\mathbf{q}}}_i}{\partial \mathbf{q}_i} \tag{59}$$

DOI: 10.1002/nme

which leads to

$$\frac{\partial \dot{\mathbf{p}}'_i}{\partial \mathbf{p}'_i} = -\frac{\partial \dot{\tilde{\mathbf{q}}}_i}{\partial \mathbf{q}_i} - 3\xi_c \tag{60}$$

We also assume that $\dot{\xi}_c$ is independent of ξ_c, i.e.

$$\frac{\partial \dot{\xi}_c}{\partial \xi_c} = 0 \tag{61}$$

By substituting Equations (57), (60), and (61) into Equation (56), we obtain

$$\sum_c \frac{\mathrm{d}f_c}{\mathrm{d}t} = \sum_c 3n_c \xi_c f_c \tag{62}$$

This leads to

$$\sum_c \left(\frac{\mathrm{d}}{\mathrm{d}t} \left(H_c^* + \frac{1}{2}\Theta_c \xi_c^2 \right) + \frac{1}{\beta_c} \frac{\mathrm{d}}{\mathrm{d}t} \log f_c \right) = 0 \tag{63}$$

where $\beta_c = (k_\mathrm{B} T_c)^{-1}$.

A possible solution for the distribution function in each cell-ensemble will be

$$f_c(\mathbf{q}, \mathbf{p}', \xi_c, t) = C \exp\left[-\beta_c \left(H_c^* + \frac{1}{2}\Theta_c \xi_c^2 \right) \right] \tag{64}$$

where C is an arbitrary constant. We then conclude that the proposed MS-NEMD algorithm does indeed produce a canonical non-equilibrium thermodynamics (e.g. [62, 63]), which is superior to the algorithm proposed in [49]. Moreover, one of the main advantages of the proposed MS-NEMD algorithm is that it will make the simulated system automatically and spontaneously return to an equilibrium state when all external forces and fluxes disappear, because in this case the MS-NEMD algorithm degenerates to a Nosé–Hoover canonical equilibrium MD algorithm.

4. THE COARSE-GRAINED MODEL

In this section, we discuss the coarse-grained thermodynamics model that is part of the MS-NEMD algorithm. How to construct an accurate coarse-grained thermodynamics model is a challenging subject [57, 64, 65]. Since the objective of this work is to formulate and implement a MS-NEMD model, the choice of the coarse-grained model is flexible. Therefore, in this work, we adopt a class of coarse-grained thermodynamics models that are based on the free-energy minimization, e.g. [66–68], and more recently [69]. Such coarse-grained models have been extensively used in practical computations for studying defects in solids. There are two main assumptions or

DOI: 10.1002/nme

approximations involved in this class of coarse-grained thermodynamics models: (1) harmonic approximation and (2) the Cauchy–Born rule. By doing so, the quantum statistical thermodynamics can be made well versed with the continuum thermodynamics [70, 71].

We consider a general three-dimensional (3D) solid with a Bravais lattice structure. We choose the zero-temperature equilibrium configuration as the reference configuration, and denote the i-th atom's position as $\mathbf{X}_i$. Since at the finite temperature, each atom is vibrating around its equilibrium position, its current position is denoted as

$$\mathbf{x}_i = \mathbf{q}_i + \mathbf{X}_i \tag{65}$$

To emphasize that $\mathbf{x}_i$ is an atom position, we denote $\mathbf{q}_i = \mathbf{u}_i$ and use

$$\mathbf{x} = \mathbf{u} + \mathbf{X} \tag{66}$$

for all material as well as configurational points that may or may not be attached with a mass.

For multiscale analysis,

$$\mathbf{u} = \bar{\mathbf{u}} + \mathbf{u}' \quad \text{and} \quad \mathbf{x} = \bar{\mathbf{x}} + \mathbf{x}' \tag{67}$$

where $\bar{\mathbf{u}}$ is defined in (8) by FE interpolation, and

$$\bar{\mathbf{x}} = \bar{\mathbf{u}} + \mathbf{X}. \tag{68}$$

The main approximation or provision of the classical Cauchy–Born rule is that within a local region, the deformation gradient is assumed to be a constant and the underlying atomic lattice will deform the same way [72]. In [49], the local ensemble is chosen as a FE and the coarse-grained thermodynamics model is formulated within each FE by using linear FE interpolation functions, such that

$$\bar{\mathbf{F}}^e = \left.\frac{\partial \bar{\mathbf{x}}}{\partial \mathbf{X}}\right|_{\forall \mathbf{X} \in \Omega_e} = \text{const.} \quad \text{and} \quad \bar{\mathbf{r}}_{i\alpha} = \bar{\mathbf{F}}^e \cdot \mathbf{R}_{i\alpha} \tag{69}$$

where $\bar{\mathbf{F}}^e$ is the coarse scale deformation gradient in the element e, $\bar{\mathbf{r}}_{i\alpha}$ denotes the coarse scale projection of the position vector between atoms i and α in the deformed lattice, $\mathbf{R}_{i\alpha}$ denotes the original bond vector in the referential space, and Ω_e denotes the domain of the element e.

In this paper, we formulate the coarse-grained model within each cell-ensemble instead of within each element, because one of the basic assumptions of the proposed MS-NEMD algorithm is that within the time scale of the coarse grain each cell-ensemble can reach to a local equilibrium state, which means that the temperature is a constant in a cell-ensemble rather than in an element, see Figure 3. Another setback of element formulation is that the temperature is always non-uniform in an element even if linear FE shape function is used to interpolate temperature field.

To use the Cauchy–Born rule in a Voronoi cell-ensemble c where the deformation is not homogeneous, we consider the local mean field. Let the FE node inside the Voronoi cell-ensemble c be labeled as I. The average coarse scale deformation gradient in the cell-ensemble c is defined as:

$$\langle \bar{\mathbf{F}} \rangle_{\Omega_c} = \left\langle \frac{\partial \bar{\mathbf{x}}}{\partial \mathbf{X}} \right\rangle_{\Omega_c} \tag{70}$$

DOI: 10.1002/nme

where Ω_c denotes the volume of the cell-ensemble c. Similarly, the average total deformation gradient in the cell-ensemble c can be defined as:

$$\langle \mathbf{F} \rangle_{\Omega_c} = \left\langle \frac{\partial \mathbf{x}}{\partial \mathbf{X}} \right\rangle_{\Omega_c} = \left\langle \frac{\partial \bar{\mathbf{x}}}{\partial \mathbf{X}} \right\rangle_{\Omega_c} + \left\langle \frac{\partial \mathbf{u}'}{\partial \mathbf{X}} \right\rangle_{\Omega_c} = \langle \bar{\mathbf{F}} \rangle_{\Omega_c} + \left\langle \frac{\partial \mathbf{u}'}{\partial \mathbf{X}} \right\rangle_{\Omega_c} \tag{71}$$

Assume that on the boundary of each cell-ensemble the following fine scale displacement flux condition holds or approximately holds,

$$\int_{\partial \Omega_c} u_i' \mathcal{N}_J \, \mathrm{d}S = 0 \tag{72}$$

where $\partial \Omega_c$ denotes the boundary of the cell-ensemble c and $\mathcal{N}_J$ are the out-normal components of $\partial \Omega_c$. This assumption leads to

$$\left\langle \frac{\partial u_i'}{\partial X_J} \right\rangle_{\Omega_c} = \frac{1}{\Omega_c} \int_{\Omega_c} \frac{\partial u_i'}{\partial X_J} \, \mathrm{d}\Omega = \frac{1}{\Omega_c} \int_{\partial \Omega_c} u_i' \mathcal{N}_J \, \mathrm{d}S = 0. \tag{73}$$

It is then straightforward that

$$\langle \mathbf{F} \rangle_{\Omega_c} = \langle \bar{\mathbf{F}} \rangle_{\Omega_c} \tag{74}$$

i.e. the average deformation gradient in a cell-ensemble equals the average coarse scale deformation gradient in the cell-ensemble. We now postulate the following coarse scale Cauchy–Born rule

$$\boxed{\bar{\mathbf{r}}_{i\alpha} = \langle \bar{\mathbf{F}} \rangle_{\Omega_c} \cdot \mathbf{R}_{i\alpha}} \tag{75}$$

Remark 1

(1) In this paper, we use $\bar{\mathbf{F}}^{\mathrm{c}}$ denoting the average coarse scale deformation gradient within a cell-ensemble c, which is approximated as the value of the coarse scale deformation gradient evaluated at the nodal point I since the cell-ensemble c contains only one nodal point I (I and c have the one-to-one correspondence). Moreover, if the linear FE interpolation functions are used,

$$\bar{\mathbf{F}}^{\mathrm{c}} := \langle \bar{\mathbf{F}} \rangle_{\Omega_c} = \bar{\mathbf{F}}(\mathbf{X}_I) = \frac{1}{\Omega_c} \sum_{e=1}^{n} \bar{\mathbf{F}}^{\mathrm{e}} w_e \tag{76}$$

where $w_e = \Omega_e \bigcap \Omega_c$ and n is the number of elements sharing the FE node I.

(2) The postulate assumption (72) may be understood in the sense of

$$\left\langle \int_{\partial \Omega_c} u_i' \mathcal{N}_J \, \mathrm{d}S \right\rangle_{\Delta t^{\mathrm{c}}} = 0. \tag{77}$$

That is valid in the sense of time average over a coarse scale time step, Δt^{c}.

To formulate the coarse-grained formulation, we first write the total potential energy of a Voronoi cell-ensemble c as

$$U_0 = \frac{1}{2} \sum_{i=1}^{n_c} \sum_{\alpha=1}^{n_b} \varphi(r_{i\alpha}) \tag{78}$$

DOI: 10.1002/nme

where n_c is the total number of atoms in the cell-ensemble c, n_b is the total number of pair atomistic bonds in a unit cell, e.g. $n_b=6$ for a hexagonal lattice, and $r_{i\alpha}=|\mathbf{r}_{i\alpha}|$ is the length of the position vector. For the multiscale Cauchy–Born rule, we state that U_0 *is approximated as the function of the mean value of the deformation gradient within the cell-ensemble*, i.e.

$$U_0(r_{i\alpha}) \approx U_0(\bar{r}_{i\alpha}) = U_0(\bar{\mathbf{F}}^{\mathrm{c}}) \tag{79}$$

where $\bar{r}_{i\alpha}=|\bar{\mathbf{r}}_{i\alpha}|$, which is related to $\bar{\mathbf{F}}^{\mathrm{c}}$ by Equation (75).

Based on the harmonic approximation [67, 68] and the Cauchy–Born rule [66, 69, 73, 74], the coarse-grained Helmholtz free energy in a cell-ensemble c may be written as

$$\mathscr{F}^{\mathrm{c}}(\bar{\mathbf{F}}^{\mathrm{c}}, T_c) = U_0(\bar{\mathbf{F}}^{\mathrm{c}}) + k_{\mathrm{B}} T_c \sum_{i=1}^{n_c} \sum_{k=1}^{3} \log\left[2\sinh\left(\frac{\hbar\omega_{ik}(\bar{\mathbf{F}}^{\mathrm{c}})}{4\pi k_{\mathrm{B}} T_c}\right)\right] \tag{80}$$

where $\hbar$ is Planck's constant divided by 2π, T_c is the kinetic temperature for the cell-ensemble c, and ω_{ik} are three normal mode frequencies for the atom i. ω_{ik} depends on $\bar{\mathbf{F}}^{\mathrm{c}}$ through $\bar{\mathbf{r}}_{i\alpha}$. It is possible to compute ω_{ik} for some simple type of lattices, e.g. an 1D lattice with identical atoms and quadratic potentials. For a general 3D lattice, one simple way to compute ω_{ik} is to adopt the local harmonic approximation [69]:

$$\left| m_i \omega_{ik}^2 \mathbb{I}^{3\times 3} - \frac{\partial^2 U_0}{\partial \mathbf{x}_i \partial \mathbf{x}_i} \right| = 0, \quad i = 1, \ldots, n_c. \tag{81}$$

Note that at the beginning of each fine scale time integration cycle, we set the kinetic temperature T_c as the coarse scale thermodynamics temperature at the FE node I. At the end of each fine scale time integration cycle, T_c is updated based on the fine scale momentums or the peculiar velocities in the cell c:

$$T_c = \frac{2}{3(n_c-1)k_{\mathrm{B}}} \left\langle \sum_{i=1}^{n_c} \frac{\mathbf{p}_i' \cdot \mathbf{p}_i'}{2m_i} \right\rangle. \tag{82}$$

A detailed implementation of the proposed MS-NEMD algorithm is described in Section 5.

With the free-energy expression $\mathscr{F}^{\mathrm{c}}$ available, one can derive the expression for entropy S^{c} at the coarse scale level for each nodal point. Recall that each cell-ensemble has only one nodal point, so the numbering of the nodal point and the numbering of the cell-ensemble are the same. We have

$$\begin{aligned} S^{\mathrm{c}} = -\frac{\partial \mathscr{F}^{\mathrm{c}}}{\partial T_c} &= \frac{\hbar}{4\pi T_c} \sum_{i=1}^{n_c} \sum_{k=1}^{3} \omega_{ik}(\bar{\mathbf{F}}^{\mathrm{c}}) \coth\left(\frac{\hbar\omega_{ik}(\bar{\mathbf{F}}^{\mathrm{c}})}{4\pi k_{\mathrm{B}} T_c}\right) \\ &\quad - k_{\mathrm{B}} \sum_{i=1}^{n_c} \sum_{k=1}^{3} \log\left[2\sinh\left(\frac{\hbar\omega_{ik}(\bar{\mathbf{F}}^{\mathrm{c}})}{4\pi k_{\mathrm{B}} T_c}\right)\right]. \end{aligned} \tag{83}$$

Similarly, we can find the internal energy E^{c} as

$$E^{\mathrm{c}} = \mathscr{F}^{\mathrm{c}} + T_c S^{\mathrm{c}} = U_0(\bar{\mathbf{F}}^{\mathrm{c}}) + \frac{\hbar}{4\pi} \sum_{i=1}^{n_c} \sum_{k=1}^{3} \omega_{ik}(\bar{\mathbf{F}}^{\mathrm{c}}) \coth\left(\frac{\hbar\omega_{ik}(\bar{\mathbf{F}}^{\mathrm{c}})}{4\pi k_{\mathrm{B}} T_c}\right). \tag{84}$$

DOI: 10.1002/nme

Based on the Helmholtz free energy $\mathscr{F}^{\mathrm{c}}$, the expression for the first Piola–Kirchhoff stress $\mathbf{P}^{\mathrm{c}}$ can be written as:

$$\mathbf{P}^{\mathrm{c}}(\bar{\mathbf{F}}^{\mathrm{c}}, T_c) = \frac{1}{\Omega_c}\frac{\partial \mathscr{F}^{\mathrm{c}}}{\partial \bar{\mathbf{F}}^{\mathrm{c}}} = \frac{1}{\Omega_c}\left\{\frac{1}{2}\sum_{i=1}^{n_c}\sum_{\alpha=1}^{n_b}\varphi'(\bar{r}_{i\alpha})\frac{\bar{\mathbf{r}}_{i\alpha}\otimes\mathbf{R}_{i\alpha}}{\bar{r}_{i\alpha}} + \frac{\hbar}{4\pi}\sum_{i=1}^{n_c}\sum_{k=1}^{3}\left[\coth\left(\frac{\hbar\omega_{ik}(\bar{\mathbf{F}}^{\mathrm{c}})}{4\pi k_{\mathrm{B}}T_c}\right)\sum_{\alpha=1}^{n_b}\omega'_{ik}(\bar{r}_{i\alpha})\frac{\bar{\mathbf{r}}_{i\alpha}\otimes\mathbf{R}_{i\alpha}}{\bar{r}_{i\alpha}}\right]\right\} \tag{85}$$

The specific heat at constant volume C_V^{c} and the specific heat at constant temperature $\mathbf{C}_T^{\mathrm{c}}$ can be derived as well:

$$C_V^{\mathrm{c}}(\bar{\mathbf{F}}^{\mathrm{c}}, T_c) = -T_c\frac{\partial^2 \mathscr{F}^{\mathrm{c}}}{\partial T_c^2} = \frac{\hbar^2}{16\pi^2 k_{\mathrm{B}}T_c^2}\sum_{i=1}^{n_c}\sum_{k=1}^{3}\frac{\omega_{ik}^2(\bar{\mathbf{F}}^{\mathrm{c}})}{\sinh^2\left(\dfrac{\hbar\omega_{ik}(\bar{\mathbf{F}}^{\mathrm{c}})}{4\pi k_{\mathrm{B}}T_c}\right)} \tag{86}$$

and

$$\mathbf{C}_T^{\mathrm{c}}(\bar{\mathbf{F}}^{\mathrm{c}}, T_c) = -T_c\frac{\partial^2 \mathscr{F}^{\mathrm{c}}}{\partial T_c \partial \bar{\mathbf{F}}^{\mathrm{c}}} = \frac{-\hbar^2}{16\pi^2 k_{\mathrm{B}}T_c}\sum_{i=1}^{n_c}\sum_{k=1}^{3}\left[\frac{\omega_{ik}(\bar{\mathbf{F}}^{\mathrm{c}})}{\sinh^2\left(\frac{\hbar\omega_{ik}(\bar{\mathbf{F}}^{\mathrm{c}})}{4\pi k_{\mathrm{B}}T_c}\right)}\sum_{\alpha=1}^{n_b}\omega'_{ik}(\bar{r}_{i\alpha})\frac{\bar{\mathbf{r}}_{i\alpha}\otimes\mathbf{R}_{i\alpha}}{\bar{r}_{i\alpha}}\right] \tag{87}$$

To find the initial guess or prediction for thermal conductivity $\mathbf{K}_T^{\mathrm{c}}$, we exploit the result from the kinetic theory [75]:

$$\mathbf{K}_T^{\mathrm{c}} = \tfrac{1}{3}C_V^{\mathrm{c}} v\ell\mathbb{I}^{3\times 3} \tag{88}$$

where v is the average particle velocity and ℓ is the particle mean free path. For non-conducting crystalline materials, we have

$$\ell = v\tau \tag{89}$$

where τ is the collision time. The values of both ℓ may be obtained from standard references, e.g. [75]. Since we assume that $C_V^{\mathrm{c}} = C_V^{\mathrm{c}}(\bar{\mathbf{F}}^{\mathrm{c}}, T_c)$, we can write $\mathbf{K}_T^{\mathrm{c}}$ as:

$$\mathbf{K}_T^{\mathrm{c}} = \mathbf{K}_T^{\mathrm{c}}(\bar{\mathbf{F}}^{\mathrm{c}}, T_c)$$

Note that in the proposed MS-NEMD algorithm, all the transport coefficients can be later updated based on the fine scale computation via the response theory. Now, we have derived the expressions for $\mathbf{P}^{\mathrm{c}}$, $\mathbf{C}_T^{\mathrm{c}}$, C_V^{c}, and $\mathbf{K}_T^{\mathrm{c}}$, and all of them can be expressed as functions of $\bar{\mathbf{F}}^{\mathrm{c}}$ and T_c.

Our coarse-grained model is built in conjunction with the FE method. To establish FE Galerkin weak formulation, we first discuss the governing equations at coarse scale level. The governing equations at the coarse scale level are: (1) the equation of motion and (2) the first law of thermodynamics. The equation of motion for finite deformations in a continuum can be written as [76]:

$$\nabla_{\mathbf{X}}\cdot\mathbf{P} + \rho_0\mathscr{B} = \rho_0\ddot{\mathbf{u}} \quad \forall\mathbf{X}\in\Omega_0 \tag{90}$$

DOI: 10.1002/nme

where $\bar{\mathbf{u}}$ is the coarse scale displacement field, $\mathbf{P}$ is the first Piola–Kirchhoff stress, ρ_0 is the density in material configuration, $\mathscr{B}$ is the body force, $\nabla_{\mathbf{X}} := \partial/\partial X_I \mathbf{E}_I$ is the material divergence operator, and Ω_0 denotes the coarse scale domain.

The equation of thermodynamic first law is expressed as [77]:

$$\dot{w} = \rho_0 z - \nabla_{\mathbf{X}} \cdot \mathbf{Q} + \mathbf{P} : \dot{\bar{\mathbf{F}}} \tag{91}$$

where w is the internal energy per unit reference volume, z is the heat source per unit mass, $\mathbf{Q}$ is the Piola–Kirchhoff heat flux, and

$$\bar{\mathbf{F}} = \mathbb{I}^{3\times 3} + \frac{\partial \bar{\mathbf{u}}}{\partial \mathbf{X}}. \tag{92}$$

To explore the meaning of Equation (91), we write the left-hand side of (91) for each cell-ensemble,

$$\begin{aligned}
\dot{w}^{\mathrm{c}} &= \frac{\dot{E}^{\mathrm{c}}}{\Omega_c} = \frac{1}{\Omega_c}\frac{\partial E^{\mathrm{c}}}{\partial \bar{\mathbf{F}}^{\mathrm{c}}} \cdot \dot{\bar{\mathbf{F}}}^{\mathrm{c}} + \frac{1}{\Omega_c}\frac{\partial E^{\mathrm{c}}}{\partial T_c}\dot{T}_c \\
&= \frac{1}{\Omega_c}\frac{\partial \mathscr{F}^{\mathrm{c}}}{\partial \bar{\mathbf{F}}^{\mathrm{c}}} \cdot \dot{\bar{\mathbf{F}}}^{\mathrm{c}} + \frac{T_c}{\Omega_c}\frac{\partial S^{\mathrm{c}}}{\partial \bar{\mathbf{F}}^{\mathrm{c}}} \cdot \dot{\bar{\mathbf{F}}}^{\mathrm{c}} + \frac{1}{\Omega_c}\frac{\partial E^{\mathrm{c}}}{\partial T_c}\dot{T}_c \\
&= \mathbf{P}^{\mathrm{c}} : \dot{\bar{\mathbf{F}}}^{\mathrm{c}} + \frac{\mathbf{C}_T^{\mathrm{c}}}{\Omega_c} : \dot{\bar{\mathbf{F}}}^{\mathrm{c}} + \frac{C_V^{\mathrm{c}}}{\Omega_c}\dot{T}_c
\end{aligned} \tag{93}$$

Equation (93) can be extended to the whole coarse scale domain Ω_0,

$$\dot{w} = \mathbf{P} : \dot{\bar{\mathbf{F}}} + \frac{\mathbf{C}_T}{\Omega_0} : \dot{\bar{\mathbf{F}}} + \frac{C_V}{\Omega_0}\dot{T} \tag{94}$$

by defining

$$\mathbf{P}(\mathbf{X}) := \sum_{c=1}^{n_{\mathrm{cell}}} \mathbf{P}^{\mathrm{c}} \chi(\Omega_c) \tag{95}$$

$$\mathbf{C}_T(\mathbf{X}) := \sum_{c=1}^{n_{\mathrm{cell}}} \frac{\Omega_0}{\Omega_c} \mathbf{C}_T^{\mathrm{c}} \chi(\Omega_c) \tag{96}$$

$$C_V(\mathbf{X}) := \sum_{c=1}^{n_{\mathrm{cell}}} \frac{\Omega_0}{\Omega_c} C_V^{\mathrm{c}} \chi(\Omega_c) \tag{97}$$

Note that $n_{\mathrm{cell}} = n_{\mathrm{node}}$, and $\chi(\Omega_c)$ is the characteristic function of each cell,

$$\chi(\Omega_c) := \begin{cases} 1 & \forall \mathbf{X} \in \Omega_c \\ 0 & \forall \mathbf{X} \notin \Omega_c \end{cases} \tag{98}$$

For the heat flux $\mathbf{Q}$, we exploit Fourier's law in the material configuration,

$$\mathbf{Q} = -\mathbf{K} \cdot \nabla_{\mathbf{X}} T \tag{99}$$

DOI: 10.1002/nme

where

$$\mathbf{K}(\mathbf{X}) := \sum_{c=1}^{n_{\text{cell}}} \mathbf{K}_T^c \chi(\Omega_c) \tag{100}$$

The final expression for the first law is obtained by substituting (94) and (99) into (91):

$$\frac{\mathbf{C}_T}{\Omega_0} : \dot{\bar{\mathbf{F}}} + \frac{C_V}{\Omega_0} \dot{T} = \rho_0 z + \nabla_{\mathbf{X}} \mathbf{F}^{-1} \cdot \mathbf{K} \cdot \mathbf{F}^{-\mathrm{T}} \nabla_{\mathbf{X}} T. \tag{101}$$

Note that the coarse scale displacement field, $\bar{\mathbf{u}}(\mathbf{X})$, and the thermodynamic temperature field, $T(\mathbf{X})$, are the primary variables governed by Equations (90) and (101) as well as the boundary and initial conditions. Consider the boundary conditions of the coarse scale problem as

$$\bar{\mathbf{u}}(\mathbf{X}) = \hat{\mathbf{u}}(\mathbf{X}) \quad \forall \mathbf{X} \in \Gamma_u \tag{102}$$

$$\mathbf{P} \cdot \mathcal{N} = \hat{\mathcal{T}}(\mathbf{X}) \quad \forall \mathbf{X} \in \Gamma_t \tag{103}$$

$$T(\mathbf{X}) = \hat{G}(\mathbf{X}) \quad \forall \mathbf{X} \in \Gamma_g \tag{104}$$

$$(J\mathbf{F}^{-1} \cdot \mathbf{K} \cdot \mathbf{F}^{-\mathrm{T}} \nabla_{\mathbf{X}} T) \cdot \mathcal{N} = \hat{H}(\mathbf{X}) \quad \forall \mathbf{X} \in \Gamma_h \tag{105}$$

where $\hat{\mathbf{u}}$ and $\hat{G}$ are given displacement and temperature at the boundary, $\hat{\mathcal{T}}$ and $\hat{H}$ are given traction and heat flux at the boundary, $\Gamma_u \cup \Gamma_t = \Omega_0$ and $\Gamma_h \cup \Gamma_g = \Omega_0$. And consider the initial conditions as

$$\mathbf{u}(\mathbf{X})|_{t_0} = \mathbf{u}_0(\mathbf{X}) \quad \forall \mathbf{X} \in \Omega_0 \tag{106}$$

$$\dot{\mathbf{u}}(\mathbf{X})|_{t_0} = \mathbf{v}_0(\mathbf{X}) \quad \forall \mathbf{X} \in \Omega_0 \tag{107}$$

$$T(\mathbf{X})|_{t_0} = T_0(\mathbf{X}) \quad \forall \mathbf{X} \in \Omega_0 \tag{108}$$

where $\mathbf{u}_0(\mathbf{X})$, $\mathbf{v}_0(\mathbf{X})$, and $T_0(\mathbf{X})$ denote the displacement, velocity, and temperature at the initial time t_0, respectively.

The Galerkin weak forms of (90) and (101) can be established via standard procedure, which are written as:

$$\int_{\Omega_0} \rho_0 \ddot{\bar{\mathbf{u}}} \cdot \delta \bar{\mathbf{u}} \, \mathrm{d}\Omega + \int_{\Omega_0} \mathbf{P} : \delta \bar{\mathbf{F}} \, \mathrm{d}\Omega = \int_{\Omega_0} \rho_0 \mathcal{B} \cdot \delta \bar{\mathbf{u}} \, \mathrm{d}\Omega + \int_{\Gamma_t} \hat{\mathcal{T}} \cdot \delta \bar{\mathbf{u}} \, \mathrm{d}S \tag{109}$$

and

$$\int_{\Omega_0} \frac{C_V}{\Omega_0} \dot{T} \delta T \, \mathrm{d}\Omega + \int_{\Omega_0} \frac{\mathbf{C}_T}{\Omega_0} : \dot{\bar{\mathbf{F}}} \delta T \, \mathrm{d}\Omega + \int_{\Omega_0} J\mathbf{F}^{-1} \cdot \mathbf{K} \cdot \mathbf{F}^{-\mathrm{T}} \nabla_{\mathbf{X}} T \cdot (\nabla_{\mathbf{X}} \delta T) \, \mathrm{d}\Omega$$

$$= \int_{\Omega_0} \rho_0 z \delta T \, \mathrm{d}\Omega + \int_{\Gamma_h} \hat{H} \delta T \, \mathrm{d}S. \tag{110}$$

The referential domain Ω_0 is then broken into a set of elements $\{\Omega_e\}, e = 1, \ldots, n\text{elem}$. The integrals in Equations (109) and (110) are expressed as summations of integrals over Ω_e. The final form of discrete FE governing equations are as follows:

$$\mathbb{M}_c \ddot{\mathbb{d}} = \mathbb{f}^{\text{ext}} - \mathbb{f}^{\text{int}} \tag{111}$$

$$\mathbb{C}_{\mathbf{V}} \dot{\mathbb{T}} + \mathbb{C}_T \dot{\mathbb{d}} + \mathbb{K}_T \mathbb{T} = \mathbb{h}^{\text{body}} + \mathbb{h}^{\text{boun}} \tag{112}$$

DOI: 10.1002/nme

with the initial conditions

$$\mathbb{d}|_{t_0} = \{\mathbf{u}_0(\mathbf{X}_1), \ldots, \mathbf{u}_0(\mathbf{X}_I), \ldots, \mathbf{u}_0(\mathbf{X}_{n_{\text{node}}})\}^{\text{T}} \tag{113}$$

$$\dot{\mathbb{d}}|_{t_0} = \{\mathbf{v}_0(\mathbf{X}_1), \ldots, \mathbf{v}_0(\mathbf{X}_I), \ldots, \mathbf{v}_0(\mathbf{X}_{n_{\text{node}}})\}^{\text{T}} \tag{114}$$

$$\mathbb{T}|_{t_0} = \{T_0(\mathbf{X}_1), \ldots, T_0(\mathbf{X}_I), \ldots, T_0(\mathbf{X}_{n_{\text{node}}})\}^{\text{T}} \tag{115}$$

The matrices and vectors in the discrete FE governing equations of the thermal–mechanical system (111)–(112) are:

$$\mathbb{M}_c = \int_{\Omega_0} \rho_0 \mathbb{N}_u^{\text{T}} \mathbb{N}_u \, \mathrm{d}\Omega \tag{116}$$

$$\mathbb{f}^{\text{int}} = \int_{\Omega_0} \mathbb{B}_u^{\text{T}} \mathbf{P}^h \, \mathrm{d}\Omega \tag{117}$$

$$\mathbb{f}^{\text{ext}} = \int_{\Gamma_t} \mathbb{N}_u^{\text{T}} \hat{\mathscr{T}} \, \mathrm{d}S + \int_{\Omega_0} \rho_0 \mathbb{N}_u^{\text{T}} \mathscr{B} \, \mathrm{d}\Omega \tag{118}$$

$$\mathbb{C}_V = \int_{\Omega_0} \frac{C_V^h}{\Omega_0} \mathbb{N}_T^{\text{T}} \mathbb{N}_T \, \mathrm{d}\Omega \tag{119}$$

$$\mathbb{C}_T = \int_{\Omega_0} \frac{1}{\Omega_0} \mathbb{N}_T^{\text{T}} \mathbf{C}_T^h \mathbb{B}_u \, \mathrm{d}\Omega \tag{120}$$

$$\mathbb{K}_T = \int_{\Omega_0} \mathbb{B}_T{}^{\text{T}} \mathbf{K}^h \mathbb{B}_T \, \mathrm{d}\Omega \tag{121}$$

$$\mathbb{h}^{\text{body}} = \int_{\Omega_0} \rho_0 z \mathbb{N}_T^{\text{T}} \, \mathrm{d}\Omega \tag{122}$$

$$\mathbb{h}^{\text{boun}} = \int_{\Gamma_h} \hat{H} \mathbb{N}_T^{\text{T}} \, \mathrm{d}S \tag{123}$$

where $\mathbb{N}_u$ and $\mathbb{N}_T$ are shape function matrices [54, 78] for $\bar{\mathbf{u}}$ and T, $\mathbb{d}$ and $\mathbb{T}$ are nodal displacement and temperature arrays,

$$\mathbb{N}_u(\mathbf{X}) = \{N_1(\mathbf{X})\mathbb{I}^{3\times3}, \ldots, N_I(\mathbf{X})\mathbb{I}^{3\times3}, \ldots, N_{n_{\text{node}}}(\mathbf{X})\mathbb{I}^{3\times3}\}^{3\times3n_{\text{node}}}$$

$$\mathbb{N}_T(\mathbf{X}) = \{N_1(\mathbf{X}), \ldots, N_I(\mathbf{X}), \ldots, N_{n_{\text{node}}}(\mathbf{X})\}^{1\times n_{\text{node}}}$$

$$\mathbb{d} = \{\mathbf{d}_1, \ldots, \mathbf{d}_I, \ldots, \mathbf{d}_{n_{\text{node}}}\}^{\text{T}}$$

$$\mathbb{T} = \{T_1, \ldots, T_I, \ldots, T_{n_{\text{node}}}\}^{\text{T}}$$

and

$$\mathbb{B}_u := \frac{\partial \mathbb{N}_u(\mathbf{X})}{\partial \mathbf{X}}, \quad \mathbb{B}_T := [\mathbf{F}^{\text{T}}] \frac{\partial \mathbb{N}_T(\mathbf{X})}{\partial \mathbf{X}} \tag{124}$$

DOI: 10.1002/nme

and

$$\mathbf{P}^h = \sum_{I=1}^{n_{\text{node}}} N_I(\mathbf{X})\mathbf{P}_I \tag{125}$$

$$C_V^h = \sum_{I=1}^{n_{\text{node}}} N_I(\mathbf{X})C_{VI} \tag{126}$$

$$\mathbf{C}_T^h = \sum_{I=1}^{n_{\text{node}}} N_I(\mathbf{X})\mathbf{C}_{TI} \tag{127}$$

$$\mathbf{K}^h = \sum_{I=1}^{n_{\text{node}}} N_I(\mathbf{X})\mathbf{K}_{TI} \tag{128}$$

where $\mathbf{P}_I$ have been determined in each cell-ensemble, i.e. Equation (85) as $\mathbf{P}^{\text{c}}$, and $C_{VI}, \mathbf{C}_{TI}, \mathbf{K}_{TI}$ are determined in Equations (86)–(88) as C_V^{c}, $\mathbf{C}_T^{\text{c}}$, and $\mathbf{K}_T^{\text{c}}$, respectively. Note that each cell-ensemble has only one node, so the numberings I and c have one-to-one correspondence.

Equations (111) and (112) are non-linear coupled equations in terms of nodal unknowns $\mathbb{d}$ and $\mathbb{T}$. We can solve (111) and (112) to obtain the coarse scale solutions $\mathbb{d}$ and $\mathbb{T}$, whereas the fine scale fluctuation is obtained by solving Equations (44) and (45). The coupling between the coarse scale computation and the fine scale computation is described in the following section.

5. IMPLEMENTATION OF THE ALGORITHM

A main difference between the proposed MS-NEMD algorithm and other molecular dynamics algorithms is that in the proposed MS-NEMD algorithm, the fine scale model alone cannot provide statistics details. The fine scale statistical model, by which the fine scale stochastic motions are described, depends on the coarse scale mean field in the following two ways: (1) the amplitude of fine scale fluctuation is controlled by the coarse scale thermodynamic temperature $\mathbb{T}$; $\mathbb{T}$ is used to set up heat reservoirs at the beginning of each fine scale time integration cycle; the fine scale motion is driven out of the equilibrium by the coarse scale mean field instead of a prescribed or fictitious external field as in some traditional NEMD simulations, such as DOLLS or SLLOD algorithms and (2) in turn, the fine scale motion provides thermal fluctuation to the mean field; at the end of each fine scale time integration cycle, the fine scale atomistic velocities are used to update coarse scale thermodynamic temperature according to Equation (82); the fine scale atomistic displacement $\mathbb{q}$ is used to calculate the atomistic force vector $\mathbb{F}$ which is then mapped to FE nodes to obtain the internal force vector $\mathbb{f}^{\text{int}}$ for the coarse scale computation. To illustrate how to implement the MS-NEMD algorithm, a complete MS-NEMD algorithmic sequence is documented as follows. The time sequence is presented in the order of numerical integration:

1. Set up FE discretization and interpolation. Calculate multiscale projection matrices, $\mathbb{P}$ and $\mathbb{Q}$.
2. Start at coarse scale time $t_N = t_0 + N\Delta t^{\text{c}}$, where t_0 is the initial time, Δt^{c} is the coarse scale time step size, and N is the current number of coarse scale time step. $\{\mathbb{d}(t_N), \dot{\mathbb{d}}(t_N), \ddot{\mathbb{d}}(t_N), \mathbb{T}(t_N), \dot{\mathbb{T}}(t_N)\}$ are solutions obtained at t_N.
3. Set up heat reservoirs, use $\mathbb{T}(t_N) = \{T_c(t_N)\}_{c=1}^{n_{\text{node}}}$ as the temperature array in the distributed Noše–Hoover thermostat network.

DOI: 10.1002/nme

4. Start at fine scale time $t_0^{\mathrm{f}}=t_N$, with $\{\mathbf{q}(t_N),\ \dot{\mathbf{q}}'(t_N),\ \ddot{\mathbf{q}}'(t_N)\}$. Enforce the multiscale decompositions:

$$\dot{\bar{\mathbf{q}}}(t_N)=\mathbb{P}\,\dot{\mathbf{q}}(t_N)\quad\text{and}\quad\dot{\mathbf{q}}'(t_N)=\mathbb{Q}\,\dot{\mathbf{q}}(t_N)$$
$$\ddot{\bar{\mathbf{q}}}(t_N)=\mathbb{P}\,\ddot{\mathbf{q}}(t_N)\quad\text{and}\quad\ddot{\mathbf{q}}'(t_N)=\mathbb{Q}\,\ddot{\mathbf{q}}(t_N)$$

5. Do $n=0:ncyl$
Update MD solutions $\{\mathbf{q},\ \dot{\mathbf{q}}',\ \ddot{\mathbf{q}}'\}$ from t_n^{f} to t_{n+1}^{f}, where $t_n^{\mathrm{f}}=t_N+n\Delta t^{\mathrm{f}}$, Δt^{f} is the fine scale time step size, n is the current number of fine scale time step, and $ncyl$ is the total number of fine scale time step. In a cell-ensemble c, atoms are associated with a heat reservoir of $T_c(t_N)$. The velocity Verlet algorithm for Nośe–Hoover chain dynamics [35, 79–81] is adopted for the MD update in each cell-ensemble c.

Part 1: Advance $\dot{\mathbf{q}}_c'$, ξ_{2k-1}, and $\dot{\xi}_{2k}$ from t_n^{f} to $t_{n+1/2}^{\mathrm{f}}$, where $k=1,\ldots,M/2$, M is the length of Nośe–Hoover chain, and $\dot{\mathbf{q}}_c'$ denotes the subvector of $\dot{\mathbf{q}}'$, i.e. the fine scale velocities of the atoms in the cell-ensemble c. Also define $\mathbb{M}_{A,c}$ as the submatrix of $\mathbb{M}_A$ and $\mathbb{F}_c$ as the subvector of $\mathbb{F}$.

$$\ddot{\mathbf{q}}_c'(t_n^{\mathrm{f}})=\mathbb{M}_{A,c}^{-1}\mathbb{F}_c(t_n^{\mathrm{f}})-\ddot{\bar{\mathbf{q}}}_c(t_N)$$
$$\dot{\mathbf{q}}_c'(t_{n+1/2}^{\mathrm{f}})=\left[\dot{\mathbf{q}}_c'(t_n^{\mathrm{f}})\left(1-\frac{\Delta t^{\mathrm{f}}}{4}\dot{\xi}_1(t_n^{\mathrm{f}})\right)+\frac{\Delta t^{\mathrm{f}}}{2}\ddot{\mathbf{q}}_c'(t_n^{\mathrm{f}})\right]\left(1+\frac{\Delta t^{\mathrm{f}}}{4}\dot{\xi}_1(t_n^{\mathrm{f}})\right)^{-1}$$
$$\xi_{2k-1}(t_{n+1/2}^{\mathrm{f}})=\xi_{2k-1}(t_n^{\mathrm{f}})+\frac{\Delta t^{\mathrm{f}}}{2}\dot{\xi}_{2k-1}(t_n^{\mathrm{f}})$$
$$\dot{\xi}_{2k}(t_{n+1/2}^{\mathrm{f}})=\left[\dot{\xi}_{2k}(t_n^{\mathrm{f}})\left(1-\frac{\Delta t^{\mathrm{f}}}{4}\dot{\xi}_{2k+1}(t_n^{\mathrm{f}})\right)+\frac{\Delta t^{\mathrm{f}}}{2}a_{\xi_{2k}}(t_n^{\mathrm{f}})\right]\left(1+\frac{\Delta t^{\mathrm{f}}}{4}\dot{\xi}_{2k+1}(t_n^{\mathrm{f}})\right)^{-1}$$
$$a_{\xi_1}(t_{n+1/2}^{\mathrm{f}})=\left[\sum_{i=1}^{n_c}m_i\dot{\mathbf{q}}_i'(t_{n+1/2}^{\mathrm{f}})\cdot\dot{\mathbf{q}}_i'(t_{n+1/2}^{\mathrm{f}})-3n_ck_{\mathrm{B}}T_c(t_N)\right]\Big/\,Q_1$$
$$a_{\xi_{2k-1}}(t_{n+1/2}^{\mathrm{f}})=\frac{Q_{2k-2}\dot{\xi}_{2k-2}^2(t_{n+1/2}^{\mathrm{f}})-k_{\mathrm{B}}T_c(t_N)}{Q_{2k-1}}$$

Part 2: Advance $\mathbf{q}_c$, ξ_{2k}, and $\dot{\xi}_{2k-1}$ at t_n^{f} to the ones at t_{n+1}^{f}:

$$\mathbf{q}_c(t_{n+1}^{\mathrm{f}})=\mathbf{q}_c(t_n^{\mathrm{f}})+\Delta t^{\mathrm{f}}(\dot{\mathbf{q}}_c'(t_{n+1/2}^{\mathrm{f}})+\dot{\bar{\mathbf{q}}}_c(t_N))$$
$$\xi_{2k}(t_{n+1}^{\mathrm{f}})=\xi_{2k}(t_n^{\mathrm{f}})+\Delta t^{\mathrm{f}}\dot{\xi}_{2k}(t_{n+1/2}^{\mathrm{f}})$$
$$\dot{\xi}_{2k-1}(t_{n+1}^{\mathrm{f}})=\left[\dot{\xi}_{2k-1}(t_n^{\mathrm{f}})\left(1-\frac{\Delta t^{\mathrm{f}}}{2}\dot{\xi}_{2k}(t_{n+1/2}^{\mathrm{f}})\right)+\Delta t^{\mathrm{f}}a_{\xi_{2k-1}}(t_{n+1/2}^{\mathrm{f}})\right]\times\left(1+\frac{\Delta t^{\mathrm{f}}}{2}\dot{\xi}_{2k}(t_{n+1/2}^{\mathrm{f}})\right)^{-1}$$

DOI: 10.1002/nme

Calculate $\mathbb{F}_c(t^{\mathrm{f}}_{n+1})$ based on $\mathfrak{q}_c(t^{\mathrm{f}}_{n+1})$ and calculate

$$a_{\xi_{2k}}(t^{\mathrm{f}}_{n+1}) = \frac{Q_{2k-1}\dot{\xi}^2_{2k-1}(t^{\mathrm{f}}_{n+1}) - k_{\mathrm{B}}T_c(t_N)}{Q_{2k}}$$

Part 3: Advance $\dot{\mathfrak{q}}'_c$, ξ_{2k-1}, and $\dot{\xi}_{2k}$ from $t^{\mathrm{f}}_{n+1/2}$ to t^{f}_{n+1}:

$$\ddot{\mathfrak{q}}'_c(t^{\mathrm{f}}_{n+1}) = \mathbb{M}^{-1}_{A,c}\mathbb{F}_c(t^{\mathrm{f}}_{n+1}) - \ddot{\mathfrak{q}}_c(t_N)$$

$$\dot{\mathfrak{q}}'_c(t^{\mathrm{f}}_{n+1}) = \left[\dot{\mathfrak{q}}'_c(t^{\mathrm{f}}_{n+1/2})\left(1 - \frac{\Delta t^{\mathrm{f}}}{4}\dot{\xi}_1(t^{\mathrm{f}}_{n+1})\right) + \frac{\Delta t^{\mathrm{f}}}{2}\ddot{\mathfrak{q}}'_c(t^{\mathrm{f}}_{n+1})\right]\left[1 + \frac{\Delta t^{\mathrm{f}}}{4}\dot{\xi}_1(t^{\mathrm{f}}_{n+1})\right]^{-1}$$

$$\xi_{2k-1}(t^{\mathrm{f}}_{n+1}) = \xi_{2k-1}(t^{\mathrm{f}}_{n+1/2}) + \frac{\Delta t^{\mathrm{f}}}{2}\dot{\xi}_{2k-1}(t^{\mathrm{f}}_{n+1})$$

$$\dot{\xi}_{2k}(t^{\mathrm{f}}_{n+1}) = \left[\dot{\xi}_{2k}(t^{\mathrm{f}}_{n+1/2})\left(1 - \frac{\Delta t^{\mathrm{f}}}{4}\dot{\xi}_{2k+1}(t^{\mathrm{f}}_{n+1})\right) + \frac{\Delta t^{\mathrm{f}}}{2}a_{\xi_{2k}}(t^{\mathrm{f}}_{n+1})\right] \times \left[1 + \frac{\Delta t^{\mathrm{f}}}{4}\dot{\xi}_{2k+1}(t^{\mathrm{f}}_{n+1})\right]^{-1}$$

End of fine scale cycle with $\{\mathfrak{q}(t_{N+1}),\ \dot{\mathfrak{q}}'(t_{N+1}),\ \ddot{\mathfrak{q}}'(t_{N+1})\}$. Note that $ncyl \cdot \Delta t^{\mathrm{f}} = \Delta t^{\mathrm{c}}$.

6. Update (correct) coarse scale temperature based on fine scale atomistic velocities for each cell-ensemble c:

$$T_c(t_{N+1/2}) = \frac{2}{3(n_c - 1)k_{\mathrm{B}}}\left\langle \sum_{j=1}^{n_c} \frac{\mathbf{p}'_j \cdot \mathbf{p}'_j}{2m_j} \right\rangle$$

and update finite element nodal position in each cell-ensemble,

$$\mathbf{x}^c(t_N) = \frac{1}{n_c}\sum_{i=1}^{n_c} \mathfrak{q}_i$$

7. Solve FE equations for $\{\mathfrak{d}(t_{N+1}),\ \dot{\mathfrak{d}}(t_{N+1}),\ \ddot{\mathfrak{d}}(t_{N+1}),\ \mathbb{T}(t_{N+1}),\ \dot{\mathbb{T}}(t_{N+1})\}$. A mixed time integration algorithm is used in coarse scale FE update, which is pioneered by Liu and Belytschko for solving dynamic fluid–structure interaction problems [82],

$$\mathfrak{d}(t_{N+1}) = \mathfrak{d}(t_N) + \Delta t^{\mathrm{c}}\,\dot{\mathfrak{d}}(t_N) + \frac{(\Delta t^{\mathrm{c}})^2}{2}\ddot{\mathfrak{d}}(t_N)$$

$$\dot{\mathfrak{d}}(t_{N+1/2}) = \dot{\mathfrak{d}}(t_N) + \frac{\Delta t^{\mathrm{c}}}{2}\ddot{\mathfrak{d}}(t_N)$$

$$\ddot{\mathfrak{d}}(t_{N+1}) = \mathbb{M}^{-1}_c(\mathfrak{f}^{\mathrm{ext}}(t_{N+1}) - \mathfrak{f}^{\mathrm{int}}(t_{N+1}))$$

$$\dot{\mathfrak{d}}(t_{N+1}) = \dot{\mathfrak{d}}(t_{N+1/2}) + \frac{\Delta t^{\mathrm{c}}}{2}\ddot{\mathfrak{d}}(t_{N+1})$$

DOI: 10.1002/nme

$$\mathbb{T}(t_{N+1}) = \mathbb{T}(t_{N+1/2}) + \Delta t^{c}\dot{\mathbb{T}}(t_N)$$

$$\dot{\mathbb{T}}(t_{N+1}) = -\mathbb{C}_V^{-1}(\mathbb{C}_T\,\dot{\mathbf{d}}(t_{N+1}) + \mathbb{K}_T\,\mathbb{T}(t_{N+1}))$$

Update the velocity

$$\dot{\bar{\mathbf{q}}}(t_{N+1}) = \mathbb{N}\,\dot{\mathbf{d}}(t_{N+1})$$

$$\dot{\mathbf{q}}(t_{N+1}) = \dot{\bar{\mathbf{q}}}(t_{N+1}) + \dot{\mathbf{q}}'(t_{N+1})$$

Update the acceleration

$$\ddot{\bar{\mathbf{q}}}(t_{N+1}) = \mathbb{N}\,\ddot{\mathbf{d}}(t_{N+1})$$

$$\ddot{\mathbf{q}}(t_{N+1}) = \ddot{\bar{\mathbf{q}}}(t_{N+1}) + \ddot{\mathbf{q}}'(t_{N+1})$$

8. Advance coarse scale time to t_{N+1}.

6. NUMERICAL EXAMPLES

6.1. An one-dimensional wave benchmark example

To validate the proposed MS-NEMD algorithm, we have carried out several numerical examples. The first example is a problem of wave propagation along 1D lattice. The Morse potential with parameters for Aluminum is used. Nearest neighbor interaction is assumed. The expression for the potential is

$$\varphi(r_{ij}) = De^{-2\alpha(r_{ij}-r_0)} - 2De^{-\alpha(r_{ij}-r_0)} \tag{129}$$

where i and j denote two atoms. The parameters for Aluminum are [83]: $r_0 = 3.253\,\text{A}$, $\alpha = 1.1646\,\text{A}^{-1}$, $D = 0.2703\,\text{eV}$, $m_a = 26.98\,\text{amu}$. The Boltzmann constant k_B is 1.3806e-23 JK^{-1} and the Planck's constant $\hbar$ is 1.0546e-34 JS. An initial displacement is given,

$$u_0(x) = \frac{B}{B-u_a}\left(1 + b\cos\frac{2\pi x}{H}\right)\left(B\exp^{-\left(\frac{x}{\sigma}\right)^2} - u_a\right) \tag{130}$$

for $|x| \leqslant L$, where $u_a = B\exp^{-(L/\sigma)^2}$, $B = 0.8r_0$, $\sigma = 10r_0$, $H = \sigma/4$, $b = 0.1$, and $L = 5\sigma$. A domain of $[-300r_0, 300r_0]$ is simulated with a total of 60 FE elements. The fine scale region is at $[-90r_0, 90r_0]$ and has 181 atoms. There are 18 fine scale FE elements and each of them consists of 10 atoms. The coarse scale time step is $1.0\times10^{-14}\,\text{s}$ and the fine scale time step is $1.0\times10^{-15}\,\text{s}$.

Figure 6 shows the comparison of the displacement solution of the 1D wave moving out of the fine scale region via (a) bridging scale method [41] or PMMS method [48] without temperature, (b) MS-NEMD method with initial temperature $T_0 = 100\,\text{K}$, and (c) MS-NEMD method with initial temperature $T_0 = 200\,\text{K}$. One can find that the initial temperature will significantly affect the local atomic displacements, or phonon motion, which eventually affects the coarse scale displacement profile as well. In fact, one may find that as the initial temperature increases, the maximum amplitude of the displacement profile decreases as indicated in Figure 6. We believe that this is due to the facts: (1) large thermal fluctuation will assist the thermal–mechanical coupling, i.e. dependence of thermal conductivity coefficient on temperature and (2) once the mechanical work

DOI: 10.1002/nme

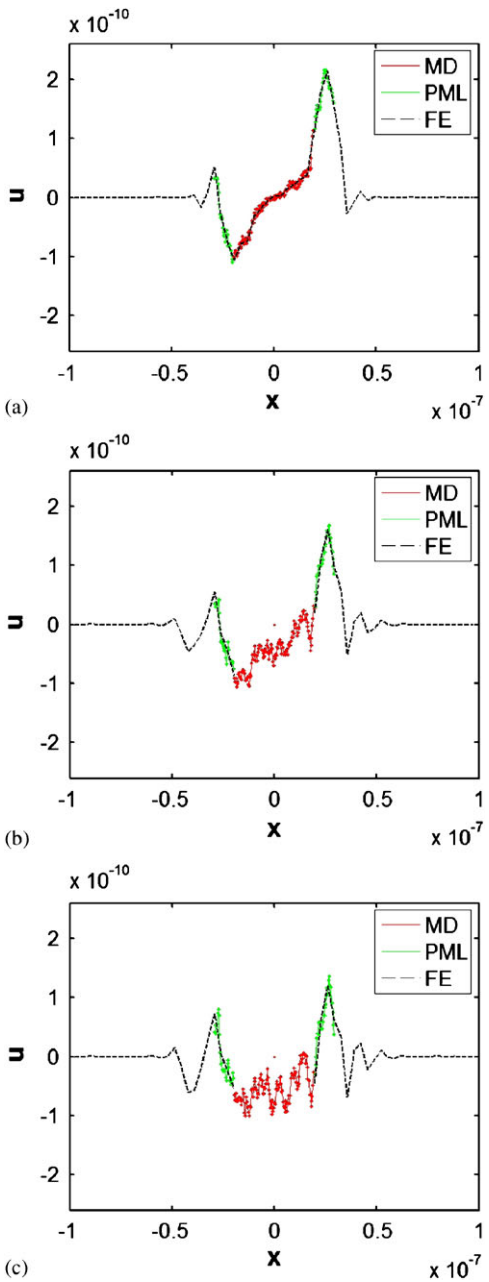

Figure 6. Displacement profiles (x and u in meter): (a) zero-temperature PMMS solution; (b) MS-NEMD solution with initial temperature $T_0 = 100\,\mathrm{K}$; and (c) MS-NEMD solution with initial temperature $T_0 = 200\,\mathrm{K}$.

DOI: 10.1002/nme

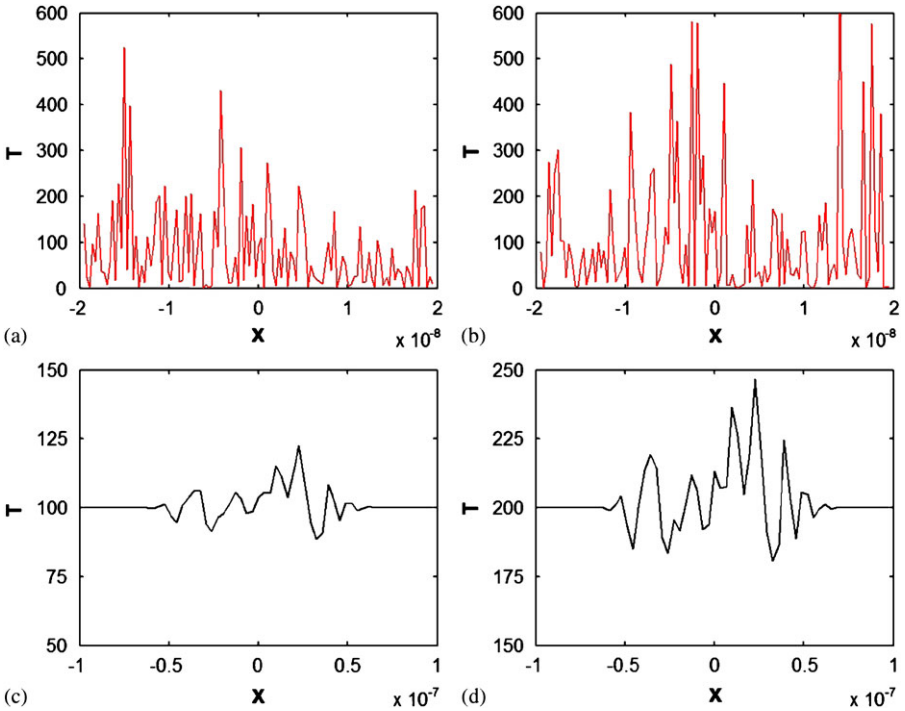

Figure 7. Temperature profiles by MS-NEMD simulation (x in meter, T in K): (a) instantaneous temperature for initial temperature $T_0 = 100\,\mathrm{K}$; (b) instantaneous temperature for initial temperature $T_0 = 200\,\mathrm{K}$; (c) coarse scale temperature for initial temperature $T_0 = 100\,\mathrm{K}$; and (d) coarse scale temperature for initial temperature $T_0 = 200\,\mathrm{K}$.

is converted into heat it tends more to diffuse out over the entire domain rather than convert back into mechanical energy again.

Moreover, the simulation results predict that the interchange of mechanical work and heat flux will generate non-uniform temperature distribution under purely non-uniform mechanical disturbance. In Figure 7, the fine scale instantaneous temperature is juxtaposed with the coarse scale thermodynamic temperature. One can observe the non-uniform temperature distribution in the fine scale region. This confirms the thermal–mechanical coupling at the both scales and their exchange between the two scales.

6.2. *An one-dimensional shock wave propagation*

The second example is the simulation of a shock wave propagation along 1D lattice. A special type of Frenkel-Kontorova potential, or the Fermi, Pasta, and Ulam (FPU)-β potential [6, 84] is used in the numerical simulation,

$$U(\mathbf{q}) = \sum_i \left(\frac{k}{2}(|q_i - q_j| - a)^2 + \frac{\mathscr{K}}{2}(q_i - a\,\mathrm{int}(q_i/a))^2 - \frac{\mathscr{K}}{24}(q_i - a\,\mathrm{int}(q_i/a))^4 \right), \quad |i-j| = 1 \quad (131)$$

E and his co-workers have used a similar potential, i.e. the first two terms of Equation (131), to simulate shock wave propagation by using the heterogeneous multiscale method [39, 40, 85]. In the

DOI: 10.1002/nme

present simulation, we use the following normalized parameters: $a=1$, $k=1$, $\mathscr{K}=0.7$, $m_a=1$, $\tilde{k}_{\mathrm{B}}=k_{\mathrm{B}}(t_c^2/m_cL_c^2)$, and $\tilde{\hbar}=\hbar(t_c/m_cL_c^2)$, where m_c, L_c, and t_c are characteristic mass, length, and time, respectively. They are chosen as: $m_c=26.98$ amu, $L_c=3.253$ A, and $t_c=2.0\times10^{-13}$ s. The function int(x) is the floor integer function that converts a real number to the next smallest integer, and it is defined as

$$\mathrm{int}(x)=n \quad \text{if and only if } n\leqslant x<n+1 \tag{132}$$

A domain of $[0, 1000]$ with 1001 atoms is considered. A strong discontinuity in displacement field (dislocation) is prescribed at $x=500$. There are 50 FE elements and each of them consists of 20 atoms. The normalized coarse scale time step is 0.1 and the normalized fine scale time step is 0.01.

We have conducted two sets of simulations. In the first set of simulations, a constant external force $f=0.04$, which is slightly higher than the critical force (the Peierls force), is applied to every atom along the 1D lattice. We use the MS-NEMD method to simulate the propagation of the dislocation, or strong discontinuity. The initial temperature in this example is chosen as $T_0=100$ K. Figure 8 shows snapshots of displacement, instantaneous kinetic (fine scale) temperature, and thermodynamic (coarse scale) temperature profiles. One can observe extreme high temperature peak moving with the shock front, which generates coarse scale heat wave propagation. Moreover, one may find that there is a good agreement between the coarse scale temperature distribution and the fine scale temperature distribution, which indicates that the definitions of temperatures used in this work are sensible. This example reveals the capacity of the MS-NEMD method to simulate a non-equilibrium process with both spatial and temporal temperature gradients.

In the second set of MS-NEMD simulations, a sub-Peierls force, $f=0.03$ is applied along the lattice. Figure 9(a–c) shows the time histories of the displacement profiles with initial temperatures $T_0=0$ K, $T_0=100$ K, and $T_0=200$ K, respectively. In Figure 9(a, b), there are stationary shock waves for every t, which indicates that the shock does not propagate along the lattice under sub-Peierls force. Whereas in Figure 9(c), we choose initial temperature $T_0=200$ K, and one can find that the shock wave starts moving from right to left, which indicates the thermal activation of shock wave or dislocation motions.

Figure 9(d–f) displays the time histories of the fine scale temperature profiles with initial temperatures $T=0$ K, $T=100$ K, and $T=200$ K, respectively. One can observe that when the initial temperature increases, the fine scale temperature distribution is visibly larger. It indicates that the thermal–mechanical interaction is more significant in the case of $T=200$ K and hence, the thermal activation of shock wave occurs when the initial temperature is increased to 200 K.

We note that first the results shown here are qualitative, because it does not correspond to any real materials, for which specific numerical simulations have to be conducted; second, similar conclusions may have been drawn based on the finite temperature equilibrium MD simulation [86]. However, in reality a shock wave only propagates in non-equilibrium states, in which both spatial and temporal temperature gradients are present and changing. To the best of the authors' knowledge, this is the first successful numerical simulation of thermal activation of 'dislocation' under non-equilibrium conditions. The fine scale calculation provides the essential source for thermal–mechanical coupling at both scales, and the activation of dislocation is clearly due to thermal fluctuations.

For the case of $f=0.03$, we have also performed the simulations by using three other different methods, i.e. (1) micro-canonical ensemble MD simulation (without temperature), (2) direct NEMD simulation (with a fixed temperature of 200 K at the boundary ends), and (3) canonical ensemble

DOI: 10.1002/nme

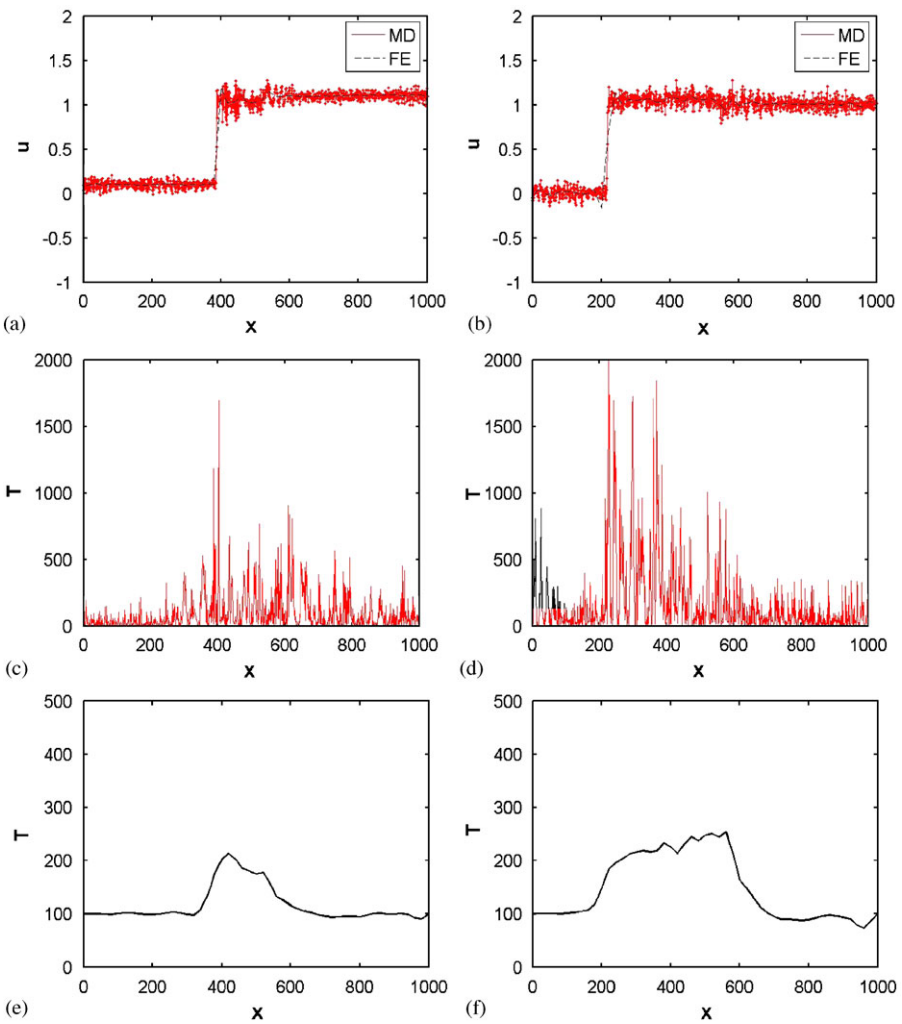

Figure 8. MS-NEMD simulation of shock wave propagation under an above-critical load $f = 0.04$: displacement profiles at (a) $t = 168$ and (b) $t = 420$; fine scale temperature profiles at (c) $t = 168$ and (d) $t = 420$; coarse scale temperature profiles at (e) $t = 168$ and (f) $t = 420$.

MD simulation (with fixed temperature of 200 K). The results are compared with that of the present MS-NEMD simulation with the initial temperature of 200 K. As shown in Figure 10(a, b), both the micro-canonical MD simulation and the direct NEMD simulation predict a stationary shock wave, which does not propagate along the lattice. Whereas in the canonical MD simulation (Figure 10(c)) and the MS-NEMD simulation (Figure 10(d)), the shock wave moves from right to left, which indicates the thermal activation of dislocation motions. From this comparison study, one can find that the micro-canonical MD simulation fails to predict thermal activation of shock wave or dislocation because it is not able to produce thermal fluctuations. The direct NEMD simulation may have failed in prediction of thermal activation of shock waves, because it uses the

DOI: 10.1002/nme

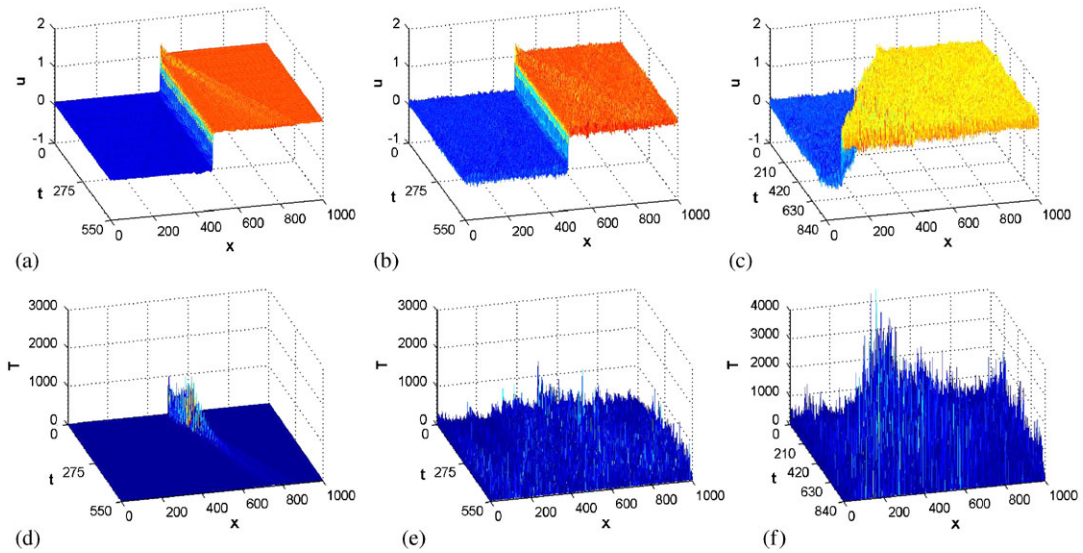

Figure 9. MS-NEMD simulation of shock wave propagation under a sub-critical load $f = 0.03$: displacement profiles with initial temperatures at (a) $T_0 = 0\,\mathrm{K}$; (b) $T_0 = 100\,\mathrm{K}$ and (c) $T_0 = 200\,\mathrm{K}$; instantaneous temperature profiles with initial temperatures at (d) $T_0 = 0\,\mathrm{K}$; (e) $T_0 = 100\,\mathrm{K}$; and (f) $T_0 = 200\,\mathrm{K}$.

micro-canonical MD in the interior of the simulation domain. On the other hand, both the equilibrium MD simulation and the MS-NEMD simulation predict the thermal activation of the dislocation, because of the intrinsic statistical or thermodynamic structures in both algorithms, which enable them to produce correct thermal fluctuations that are responsible for exciting dislocation motion or shock wave propagations. This example clearly demonstrates an advantage of the proposed MS-NEMD algorithm over the direct NEMD algorithm.

Furthermore, the instantaneous temperature profiles obtained by the four different methods are juxtaposed in Figure 11. In the micro-canonical ensemble MD simulation, no thermodynamic temperature is enforced; and in the direct NEMD simulation, only two boundary thermostats are enforced with a fixed temperature of 200 K. Subsequently, these two simulations put a constraint on kinetic energy distribution. In other words, the thermal–mechanical interaction is constrained. Therefore, the instantaneous temperature distributions obtained by the micro-canonical ensemble MD simulation (Figure 11(a)) and the direct NEMD simulation (Figure 11(b)) are visibly smaller than that of the canonical ensemble MD simulation (Figure 11(c)) and the MS-NEMD simulation (Figure 11(d)). This may explain the thermal activation of dislocation in the later two simulations. Moreover, although the displacement profile of the proposed MS-NEMD simulation is close to that of the canonical ensemble MD simulation (see Figure 10(c, d)), the MS-NEMD instantaneous temperature distribution exhibits larger fluctuations (see Figure 11(c, d)). Therefore, the proposed MS-NEMD simulation gives more sensible temperature distribution.

6.3. A two-dimensional shock wave propagation

To demonstrate the multidimensional characters of the MS-NEMD algorithm, we present simulation results of a shock wave propagation in 2D space in this subsection.

DOI: 10.1002/nme

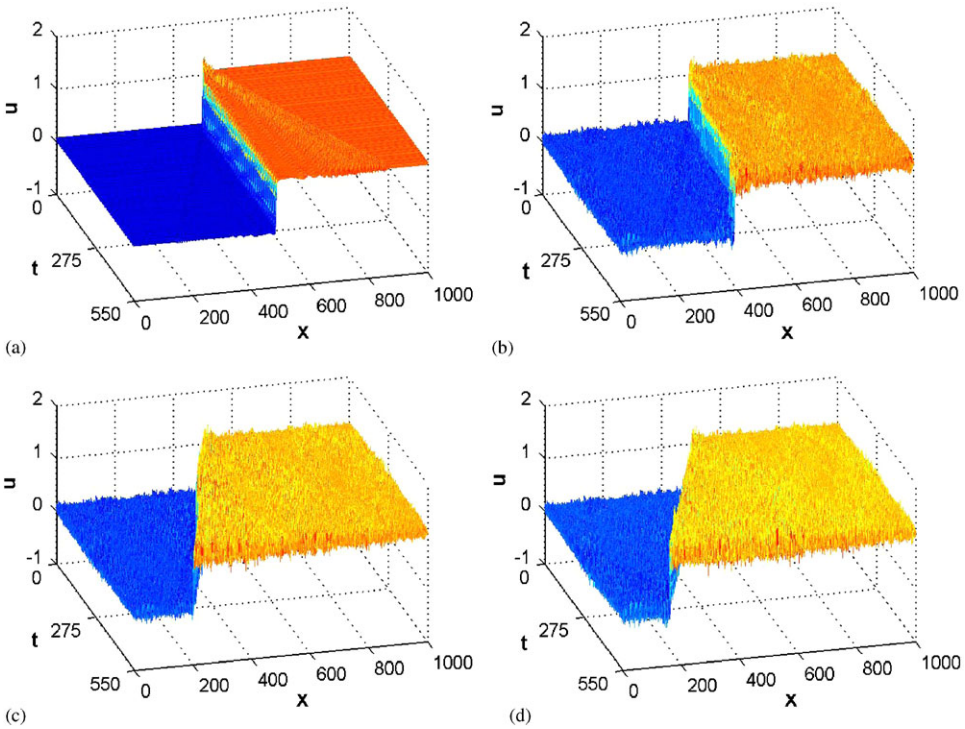

Figure 10. Shock wave propagation under a sub-critical load $f=0.03$: displacement profiles obtained by (a) micro-canonical ensemble MD simulation, (b) direct NEMD simulation, (c) canonical ensemble MD simulation (with fixed temperature), and (d) MS-NEMD simulation.

We consider a shock wave propagating in a hexagonal lattice. The dimension of the computation domain is $[-100, 100]\times[-100, 100]$. The normalized interatomic spacing is chosen to be 1. Inside the domain, there are 40 401 atoms. The coarse scale continuum is discretized into 800 triangle elements, and there are total of 441 FE nodes and each of them represents a Voronoi cell-ensemble of 100 atoms. An initial dislocation or out-of-plane displacement in x_3 direction is prescribed as: $q(r)=1.0$ for $r\leqslant 20$. A constant out-of-plane force $f=0.04$, which is slightly higher than the critical lattice friction force (the Peierls force), is applied to every atom. The FPU-β potential [6] is used as the atomistic potential,

$$U(\mathbf{q})=\sum_{i,j}\left(\frac{k}{2}(q_{i,j}-q_{m,n})^2+\frac{\mathcal{K}}{2}(q_{i,j}-\mathrm{int}(q_{i,j}))^2-\frac{\mathcal{K}}{24}(q_{i,j}-\mathrm{int}(q_{i,j}))^4\right)$$
$$|(i+j)-(m+n)|=1,\quad \text{or}\quad |i-m|=1, |j-n|=1 \tag{133}$$

where the subscript indices, i and j, denote the position of a discrete point in the 2D plane. The parameters used in computations are the same as those in the example of 1D shock wave propagation, because the deformation mode of a screw dislocation is anti-plane strain and we only have out-plane displacement component.

DOI: 10.1002/nme

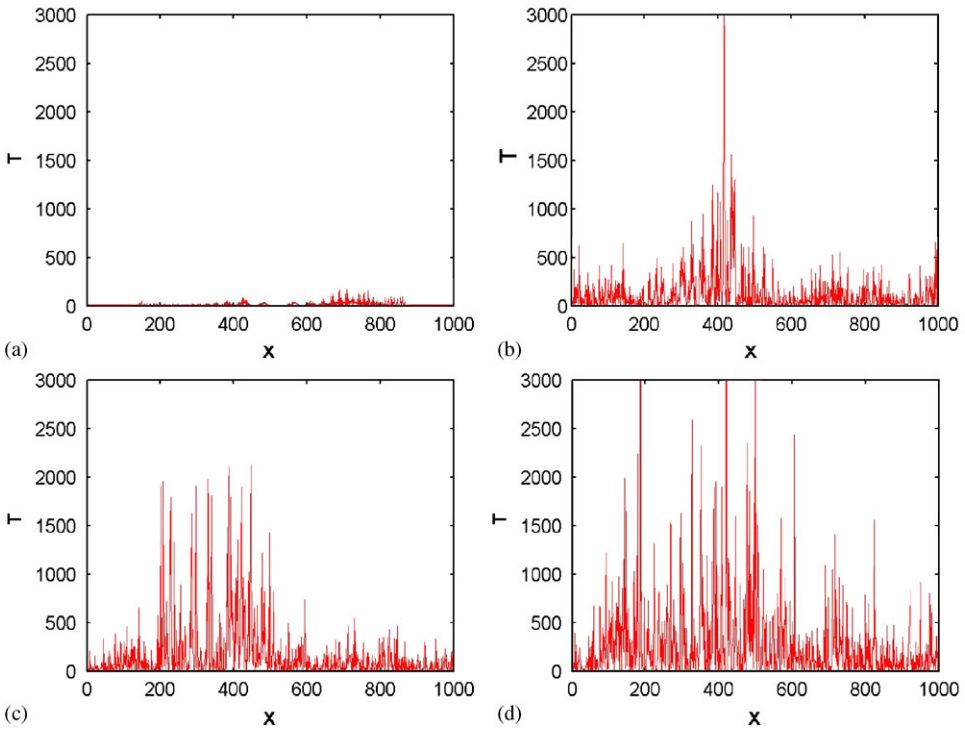

Figure 11. Shock wave propagation under a sub-critical load $f = 0.03$: instantaneous temperature profiles obtained by (a) micro-canonical ensemble MD simulation, (b) direct NEMD simulation, (c) canonical ensemble MD simulation (with fixed temperature), and (d) MS-NEMD simulation.

The normalized coarse scale time step is 0.2, and the normalized fine scale time step is 0.02. The initial temperature is chosen as $T_0 = 100\,\mathrm{K}$ that distributes uniformly throughout the domain.

A time sequence of displacement profiles obtained by the MS-NEMD simulation are shown in Figure 12(a–d). One can observe that the shock wave moves from the center to the boundaries. In Figure 12(e–h), we also show the displacement profiles obtained by the direct NEMD simulation for comparison. One may find that the results obtained by the MS-NEMD simulation show visibly larger displacement fluctuations than that of the direct NEMD simulation. Second, in Figure 13, we compare the temperature profiles obtained by the direct NEMD simulation and the MS-NEMD simulation. The MS-NEMD results indicate that the temperature amplitude in the region that shock wave passes through will not drop down to the initial temperature, and it will remain fluctuating for some time. Whereas based on the temperature profiles obtained by the direct NEMD simulation, the temperature inside the zone that shock wave passes through will immediately drop to the initial temperature. This cannot be true because the time scale for heat diffusion is much larger than the simulation time reported.

The above example had been carried out before in [87] by using the algorithm that is based on a multidimensional theory of non-equilibrium multiscale method proposed in [49]. One may compare the results below to those reported in [87].

DOI: 10.1002/nme

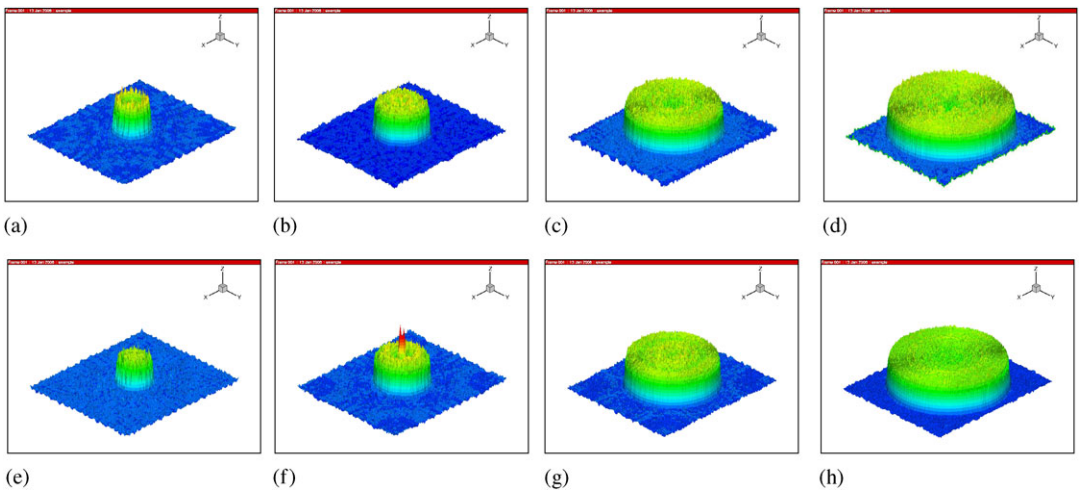

Figure 12. A 2D shock wave propagation: (a–d) a time sequence of displacement profiles obtained by MS-NEMD simulation; (e–h) a time sequence of displacement profiles obtained by direct NEMD simulation.

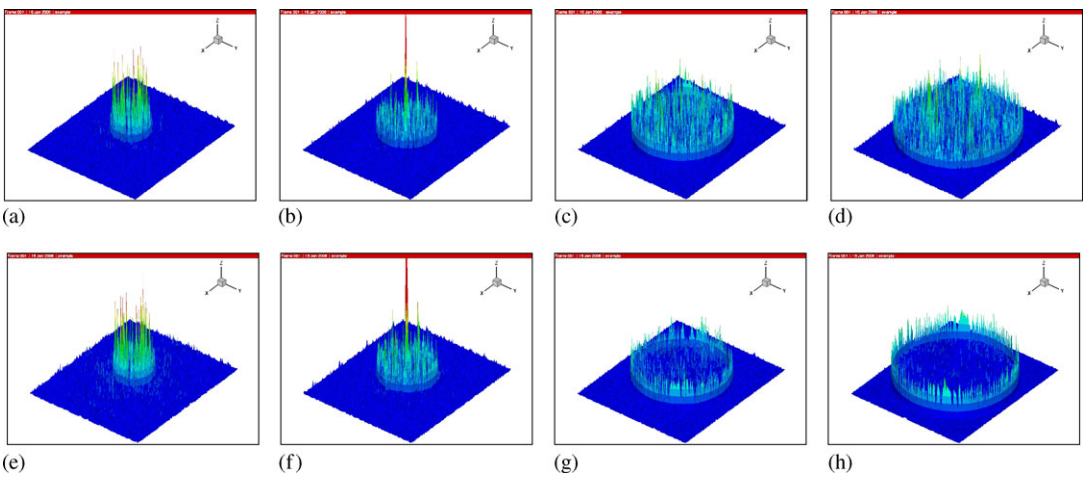

Figure 13. A 2D shock wave propagation: (a–d) a time sequence of instantaneous temperature profiles obtained by MS-NEMD simulation; (e–h) a time sequence of instantaneous temperature profiles obtained by direct NEMD simulation.

7. OUTLOOK

In this work, an MS-NEMD method has been formulated, implemented, and tested in numerical computations. It is shown that the distributed Nosé–Hoover thermostat network approach may yield a local canonical distribution function for NEMD. Using the canonical approach and the local equilibrium approach to study non-equilibrium systems is not new, and it can be traced back to

DOI: 10.1002/nme

Mori [88], Yamada and Kawasaki [89], Kawasaki and Gunton [62], and more recently Mavrantzas and Öttinger [90], Taniguchi and Morriss [63], and Edwards *et al.* [24]. In fact, the canonical distribution approach has become a powerful method to study non-equilibrium thermodynamics. The contribution of this work is to rigorously establish a local canonical distribution approach to study NEMD in a setting of concurrent multiscale coupling. Moreover, the underline principle for the distributed Nosé–Hoover thermostat network approach is to use local thermodynamic equilibrium assumption to study general non-equilibrium processes. Such philosophy and strategy have been adopted by mainstream theoretical physicists in many years. In fact, the local thermodynamic equilibrium assumption has been extensively used to construct non-equilibrium thermodynamics and non-equilibrium statistical mechanics. This work may be the first attempt to use it in multiscale analysis—This is the novelty of the work.

The proposed MS-NEMD method has the following merits:

- Different from our earlier work [49], the proposed MS-NEMD simulation is canonical;
- The distributed Nosé–Hoover thermostat network not only provides a source of random force based on mean field intensity, but also accelerates thermal relaxation by bridging time scales;
- The MS-NEMD simulation may be still locally time-reversible, which we cannot verify yet, but it is globally time-irreversible, because of (a) the coupling of the dynamics at different scales and (b) thermal–mechanical interactions among different Voronoi cell-ensembles;
- The role of the micro-level deterministic thermostats is more in assisting heat conduction or thermal relaxation than just adding or removing heat.

The potential applications of the MS-NEMD are multitude, and in the following we list a few that we think are important:

- *Accurate prediction of thermal conductivity of crystalline solids*: Recent study has shown that the conventional MD simulation of the lattice thermal conductivity have severe limitations on accuracy [91]. The main reason for such limitation is the lack of accurate description on phonon thermal transport like phonon–phonon scattering. As shown in this paper, the MS-NEMD algorithm will provide a powerful local equilibrium approach for a large class of non-equilibrium problems. Because the mutliscale non-equilibrium molecular/continuum approach can attain local equilibrium in a general non-equilibrium process, it allows us to define and measure local temperature by spatial averaging kinematic energy rather than from the original temperature definition of temporal averaging—an ergodic assumption that the micro-canonical ensemble system does not satisfy. Furthermore, the bridging scale decomposition approach leads to a global distributed COM coordinate, which allows us accurately define and measure the local peculiar velocity and hence the local temperature. Accordingly, MS-NEMD can accurately simulate phonon interactions, scattering, and phonon statistical distribution. It is expected that it may be possible that MS-NEMD may provide a means to measure thermal conductivity tensor in 3D under general non-equilibrium conditions.
- *Accurate simulation and prediction of the thermal conductance at material interfaces*: The prediction of the thermal conductance at material interfaces is another key technique component in the thermal management of integrated circuits in thin films, micro-electronic-mechanical-system (MEMS), and nano-electronic-mechanical-system (NEMS), which has been a major challenge in both simulations as well as experimental measurements [92]. As shown in this paper, MS-NEMD provides a convenient framework to accurately simulate multiscale phonon interactions and scattering. Because (1) it can clearly separate high

DOI: 10.1002/nme

frequency atomic vibrations with long range acoustic wave propagation, and therefore (2) it can capture the acoustic wave transmission, reflection, and scattering at the material interface under non-equilibrium conditions.

- *Providing accurate*, *efficient*, *and physics-based multiscale coupling algorithms*: The main challenge for the concurrent multiscale simulation is the multiscale coupling and exchange of information. The proposed MS-NEMD method is in fact a special algorithm for a very general multiscale paradigm. In this work, we have only demonstrated a local canonical ensemble approach to couple the macroscale variable *temperature* with atom vibration, in which the local temperature is enforced in each cell ensemble. We can apply the similar technique to develop a local Norton ensemble for a general non-equilibrium system, in which the macroscale stress may be enforced in each cell ensemble by a distributed local thermostat approach. By doing so, we create an accurate multiscale information passage that concurrently exchange information among different scales. This multiscale coupling paradigm for non-equilibrium systems is most general, statistically correct, and elegant approach. It will be instrumental for simulations of thermal–mechanical interaction and evolution of defects in multiscale scales, such as thermal activations of dislocations, nanoscale fracture, vacancy and solvent diffusion due to thermal–mechanical interactions, molecular simulation of turbulence flows. These processes are not only important for miniature electronic systems, but also hold the promise on studying problems, such as stress corrosion cracking, radiation damage, and high temperature creep, which are the main concerns for designing next generation of superalloys and self-healing materials.

In fact, currently we are working on applying the MS-NEMD method to simulate heat conduction and fracture in multiple dimensions. To simulate fracture, the drifting COM manifold, which is represented by FEM interpolation, has to be able to automatically adapt its evolving topological configuration. This can be accomplished by employing a multiscale cohesive zone model [93], which will be reported in a separated work [94].

We realize, nevertheless, the necessity of a systematic parametric study for the propose MS-NEMD paradigm to determine (1) a suitable size of Voronoi cell-ensemble, i.e. how many atoms should be in a Voronoi cell-ensemble. For instance, the cell-size of the MS-NEMD simulation may be determined by the length of the phonon-free-mean-path, which is a local property depending on many different factors, such as the local geometry and dimension of the solid, microstructure or inhomogeneity distribution, and defect position and its state of evolution; (2) the suitable time step for coarse scale integration; and (3) the convergence and stability of transport coefficients determined by the fine scale calculations, etc.

In fact, these issues are related to the following fundamental questions: '(*1*) *what determines the size of the coarse grains and* (*2*) *if there is arbitrariness does it have physical implications, e.g. with respect to the second law?*' [65]. Since in the multiscale formulation the temperature is calculated as the average peculiar kinetic energy in a local cell-ensemble, the system's entropy has to be dependent on the size of the cell-ensemble or the coarse grain selection. It is also related to the coarse scale time step size, because the coarse scale time step size is the duration to achieve the local equilibrium. In general, this is a challenge in multiscale calculation, because the minimum size of cell-ensemble is dictated by the phonon mean free path, which is a physical quantity that may be affected by the presence of defects. In fact, the problem on how to select the size of the coarse grain cell is NOT NEW, it has been a major technical problem in the direct NEMD simulation as well. In most direct NEMD simulations, the temperature is calculated by averaging

DOI: 10.1002/nme

kinetic energy of atoms in a finite local strip, hence the size of the strip will affect the calculation of temperature. In order to correctly calculate the temperature, most direct NEMD simulations are 3D calculations, the heat flux is usually chosen along one direction and the heat flux is assumed to be in a steady state. Therefore even though the thickness of the finite strip may be small, one may choose large sizes for the other two dimensions that are perpendicular to the direction of the heat flux so that there are still sufficient number of atoms in a 3D simulation cell so that the temperature calculation is accurate.

This strategy can be applied to the proposed MS-NEMD method as well, but it may limit the applications of MS-NEMD to 1D and 2D applications of thermo-mechanical coupling problems just like that of the direct NEMD. Even if the heat flux and temperature gradient are completely in 3D character, the MS-NEMD method proposed in this paper may still work under the Casimir limit, i.e. for the case that the size of the ensemble cell is sufficiently larger than the average phonon mean-free-path.

Another important issue is: *how to update transport coefficients based on the fine scale computations*. In the present multiscale formulation, the values of transport coefficients, such as C_V, $\mathbf{C}_T$, and $\mathbf{K}_T$ are calculated or estimated by the coarse-grained formulation, and they may only serve as the initial guess of the transport coefficients. The precise values of various transport coefficients should be obtained based on the fine scale calculations. For example, instead of using the coarse-grained approximation, $\kappa_T = \frac{1}{3} C_V v\ell$, we consider to use,

$$\kappa_T = \frac{J_{c+1} - J_c}{(T_{c+1} - T_c)/h}, \text{ etc.} \tag{134}$$

for 1D thermal–mechanical interaction problems. Currently, we are working on justification or validity of using (134) to calculate the thermal diffusion coefficients. It may be possible to develop a multiscale linear response theory to calculate transport coefficients. All these remaining issues and tasks will be discussed in subsequent papers.

ACKNOWLEDGEMENTS

The authors thank Dr Xiaohu Liu for his early participation in this work. This work is supported by a grant from NSF (CMMI-0800744), which is greatly appreciated.

REFERENCES

1. Progogine I. *Introduction to Thermodynamics of Irreversible Processes* (3rd edn). Wiley: New York, 1967.
2. Zubarev DN, Morozov V, Ropke G. *Statistical Mechanics of Nonequilibrium Processes*: *Basic Concepts*, *Kinetic Theory*. Wiley: New York, 1996.
3. Hoover WG. Canonical dynamics: equilibrium phase-space distributions. *Physical Review A* 1985; **31**:1695–1697.
4. Baranyai A. Heat flow studies for large temperature gradients by molecular dynamics simulation. *Physical Review E* 1996; **54**:6911–6917.
5. Müller-Plathe F. A simple nonequilibrium molecular dynamics method for calculating the thermal conductivity. *Journal of Chemical Physics* 1997; **106**:6082–6085.
6. Lepri S, Livi R, Politi A. Thermal conduction in classical low-dimensional lattices. *Physics Reports* 2003; **377**:1–80.
7. Poulikakos D, Arcidacono S. Molecular dynamics simulation in nanoscale heat transfer: a review. *Microscale Thermophysical Engineering* 2003; **7**:181–206.
8. Castejon HJ. Nonequilibrium molecular dynamics calculation of the thermal conductivity of solid materials. *Journal of Physics Chemistry*, *B* 2003; **107**:826–828.

DOI: 10.1002/nme

9. Tokumasu T, Kamijo K. Molecular dynamics study for the thermal conducitivy of diatomic liquid. *Superlattice and Microstructure* 2004; **35**:217–225.
10. Chantrenne P, Barrat JL. Finite size effects in determination of thermal conductivities: comparing molecular dynamics with simple models. *ASME Journal of Heat Transfer* 2004; **126**:577–585.
11. Baalss D, Hess S. Nonequilibrium molecular dynamics studies on the anisotropic viscosity of perfectly aligned nematic liquid crystals. *Physical Review Letters* 1986; **57**:86–89.
12. Kröger M, Makhloufi R. Wormlike micelles under shear flow: a microscopic model studied by nonequilibrium-molecular-dynamics simulations. *Physical Review E* 1995; **53**:2531–2536.
13. Kröger M, Hess S. Rheological evidence for a dynamical crossover in polymer melts via nonequilibrium molecular dynamics. *Physics Review Letters* 2000; **85**:1128–1131.
14. Xu L, Sedigh MG, Sahimi M, Tsotsis TT. Nonequilibrium molecular dynamics simulation of transport of gas mixtures in nanopores. *Physical Review Letters* 1998; **80**:3511–3514.
15. Jansen TIC, Snijders JG. The third- and fifth-order nonlinear Raman response of liquid CS_2 calculated using a finite field nonequilibrium dynamics method. *Journal of Chemical Physics* 2000; **113**:307–311.
16. MacElroy JMD, Boyle MJ. Nonequilibrium molecular dynamics simulation of a model carbon membrane separation of CH_4/H_2 mistures. *Chemical Engineering Journal* 1999; **74**:85–97.
17. Hoover WG. Systems far from equilibrium. In *Systems Far from Equilibrium*, Garrido L (ed.). Springer: Berlin, 1980; 373–380.
18. Hoover WG, Evans DJ, Hickman RB, Ladd AJC, Ashurst WT, Moran B. Lennar-Jones triple-point bulk and shear viscosities. Green-Kubo theory, Hamiltonian mechanics, and nonequilibrium molecular dynamics. *Physical Review A* 1980; **22**:1690–1697.
19. Hoover WG. Nonequilibrium molecular dynamics. *Annual Review of Physical Chemistry* 1983; **34**:103–127.
20. Evans DJ, Morriss GP. Nonlinear-response theory for steady planar Couette flow. *Physics Review A* 1984; **30**:1528–1530.
21. Evans DJ, Morriss GP. *Statistical Mechanics of Nonequilibrium Liquids*. Academic Press Inc: San Diego, 1990.
22. Tuckerman ME, Mundy CJ, Balasubramanian S, Klein ML. Modified nonequilibrium molecular dynamics for fluid flows with energy conservation. *Journal of Chemical Physics* 1997; **106**:5616.
23. Edwards BJ, Dressler M. A reversible problem in non-equilibrium thermodynamics: Hamiltonian evolution equations for non-equilibrium molecular dynamics simulations. *Journal of Non-Newtonian Fluid Mechanics* 2001; **96**:163–175.
24. Edwards BJ, Baig C, Keffer DJ. An examination of the validity of nonequilibrium molecular-dynamics simulation algorithms for arbitrary steady-state flows. *Journal of Chemical Physics* 2005; **123**. Article no. 1141106.
25. Edwards BJ, Baig C, Keffer DJ. A validation of the p-SLLOD equations of motion for homogeneous steady-state flows. *Journal of Chemical Physics* 2006; **124**. Article no. 194104.
26. Baig C, Edwards BJ, Keffer DJ, Cochran HD. A proper approach for nonequilibrium molecular dynamics simulations of planar elongational flow. *Journal of Chemical Physics* 2005; **122**. Article no. 114103.
27. Evans DJ. Homogeneous NEMD algorithm for thermal conductivity-application of non-canonical linear response theory. *Physics Letters* 1983; **91A**:457–460.
28. Zhang F, Isbister DJ, Evans DJ. Nonequlibrium molecular dynamics simulations of heat flow in one-dimensional lattices. *Physical Review E* 2000; **61**:3541–3546.
29. Zhang M, Lussetti E, de Souza LES, Müller-Plathe F. Thermal conductivities of molecular liquids by reverse nonequilibrium molecular dynamics. *Journal of Physical Chemistry B* 2005; **109**:15060–15067.
30. Hoover WG, Ladd AJC, Moran B. High-strain-rate plastic flow studied via nonequilibrium molecular dynamics. *Physics Review Letters* 1982; **48**:1818–1820.
31. Holian BL, Lomdahl PS. Plasticity induced by shock waves in nonequilibrium molecular-dynamics simulations. *Science* 1998; **280**:2085–2088.
32. Evans DJ, Hoover WG, Failor BH, Moran B, Ladd AJC. Nonequilibrium molecular dynamics via Gauss's principle of least constraint. *Physical Review A* 1983; **8**:1016.
33. Galea TM, Attard P. Constraint method for deriving nonequilibrium molecular dynamics equations of motion. *Physical Review E* 2002; **66**. Article No. 041207.
34. Bright JN, Evans DJ. New observations regarding deterministic, time-reversible thermostats and Gauss's principle of least constraint. *Journal of Chemical Physics* 2005; **122**. Article no. 194106.
35. Martyna GJ, Klein ML, Tuckerman ME. Noseé–Hoover chains: the canonical ensemble via continuous dynamics. *Journal of Chemical Physics* 1992; **97**:2635–2645.
36. Chen G. *Nanoscale Energy Transport Sand Conversion*. Oxford University Press: Oxford, 2005.

DOI: 10.1002/nme

37. Volz SG, Saulnier JB, Chen G, Beauchamp P. Computation of thermal conductivity of Si/Ge superlattices by molecular dynamics techniques. *Microelectronics Journal* 2000; **31**:815–819.
38. Gomes CJ, Madrid M, Goicochea JV, Amon CH. In-plane sand out-of-planr thermal conductivity of silicon thin films predicted by molecular dynamics. *ASME Journal of Heat Transfer* 2006; **128**:1114–1121.
39. E W, Huang Z. Matching conditions in atomistic-continuum modeling materials. *Physical Review Letters* 2001; **87**:135501-1-4.
40. E W, Huang Z. A dynamic atomistic-continuum method for the simulation of crystalline materials. *Journal of Computational Physics* 2002; **182**:234–260.
41. Wagner GJ, Liu WK. Coupling of atomistic sand continuum simulations using a bridging scale decomposition. *Journal of Computational Physics* 2003; **190**:249–274.
42. Wagner GJ, Karpov EG, Liu WK. Molecular dynamics boundary conditions for regular crystal lattices. *Computer Method in Applied Mechanics and Engineering* 2004; **193**:1579–1601.
43. Park HS, Karpov EG, Liu WK. Non-reflecting boundary conditions for atomistic, continuum and coupled atomistic/continuum simulations. *International Journal for Numerical Methods in Engineering* 2005; **64**: 237–259.
44. Tang Z, Zhao H, Li G, Aluru NR. Finite-temperature quasicontinuum method for multiscale analysis of silicon nanostructures. *Physical Review B* 2006; **74**. Article no. 064110.
45. Yun G, Park HS. A multiscale, finite deformation formulation for surface stress effects on the coupled thermomechanical behavior of nanomaterials. *Computer Methods in Applied Mechanics and Engineering* 2008; **197**:3337–3350.
46. Xiao SP, Belytschko T. A bridging domain method for coupling continua with molecular dynamics. *Computer Methods in Applied Mechanics and Engineering* 2004; **193**:1645–1669.
47. To A, Li S. Perfectly matched multiscale simulations. *Physics Review B* 2005; **72**. Article no. 035414.
48. Li S, Liu X, Agrawal A, To A. The perfectly matched multisclae simulation revised. *Physical Review B* 2006; **74**. Article no. 045418.
49. Liu X, Li S. Nonequilibrium multiscale computational model. *Journal of Chemical Physics* 2007; **126**. Article no. 124105.
50. Li S, Sheng N, Liu X. A non-equilibrium multiscale simulation paradigm. *Chemical Physics Letters* 2008; **451**:293–300.
51. Park HS, Karpov EG, Liu WK. A temperature equation for coupled atomistic/continuum simulations. *Computer Methods in Applied Mechanics and Engineering* 2004; **193**:1713–1732.
52. Karpov EG, Park HS, Liu WK. A phonon heat bath approach for the atomistic and multiscale simulation of solids. *International Journal for Numerical Methods in Engineering* 2007; **70**:351–378.
53. Keffer DJ, Baig C, Adhangale P, Edwards BJ. A generalized Hamiltonian-based algorithm for rigorous equilibrium molecular dynamics simulation in the canonical ensemble. *Journal of Non-Newtonian Fluid Mechanics* 2008; **152**:129–139.
54. Zienkiewicz OC, Taylor RL. *The Finite Element Method* (5th edn), vol. 1. Butterworth-Heinemann: Oxford, U.K., 2000.
55. Rudd RE, Broughton JQ. Coarse-grained molecular dynamics: nonlinear finite elements and finite temperature. *Physical Review B* 2005; **72**. Article no. 144104.
56. Qiang D, Faber V, Gunzburger M. Centroidal voronoi tesselations: application and algorithm. *SIAM Review* 1999; **41**:637–676.
57. Taniguchi T. Thermodynamical properties in nonequilibrium statistical mechanics. *Physica A* 1997; **236**:448–484.
58. Bathe KJ. *Finite Element Procedures*. Prentice-Hall: Englewood Cliffs, NJ, 1996.
59. Nosé S. A molecular dynamics method for simulations in the canonical ensemble. *Molecular Physics* 1984; **52**:255–268.
60. Nosé S. An extension of the canonical ensemble molecular dynamics method. *Molecular Physics* 1986; **57**: 187–191.
61. Liu WK, Karpov EG, Park HS. *Nano Mechanics Sand Materials*. Wiley: The Atrium, Southern Gate, Chichester, 2006.
62. Kawasaki K, Gunton D. Theory of nonlinear transport processes: nonlinear shear viscosity and normal stress effects. *Physical Review A* 1973; **8**:2048–2064.
63. Taniguchi T, Morriss G. Steady shear flow thermodynamics based on a canonical distribution approach. *Physics Review E* 2004; **70**. Article no. 056124.
64. Gaveau B, Schulman LS. Master equation based formulation of nonequilibrium statistical mechanics. *Journal of Mathematical Physics* 1996; **37**:3897–3932.

DOI: 10.1002/nme

65. Schulman LS, Gaveau B. Coarse grains: the emergence of space sand order. *Foundations of Physics* 2001; **31**:713–731.
66. Weiner JH. *Statistical Mechanics of Elasticity*. Wiley: New York, 1983.
67. LeSar R, Najafabadi R, Srolovitz DJ. Finite-temperature defect properties from free-energy minimization. *Physical Review Letters* 1989; **63**:624–627.
68. Foiles S. Evaluation of harmonic methods for calculating the free energy of defects in solids. *Physical Review B* 1994; **49**:14930–14939.
69. Jiang H, Huang Y, Hwang KC. A finite-temperature continuum theory based on interatomic potentials. *ASME Journal of Engineering Materials and Technology* 2005; **127**:408–416.
70. Silhavy M. *The Mechanics and Thermodynamics of Continuous Media*. Springer: Berlin, 1997.
71. Maugin GA. *The Thermomechanics of Nonlinear Irreversible Behaviors—An Introduction*. World Scientific: Singapore, 1999.
72. Tadmor E, Ortiz M, Phillips R. Quasicontinuum analysis of defects in solids. *Philosophycal Magazine A* 1996; **73**:1529–1563.
73. Diestler DJ. Coarse-grained description of multiple scale processes in solid systems. *Phyiscal Review B* 2002; **66**. Article no. 184104.
74. Wu ZB, Diestler DJ, Feng R, Zeng XC. Coarse-graining description of solid systems at nonzero temperature. *Journal of Computational Physics* 2003; **119**:8013–8023.
75. Kittel C. *Introduction to Solid State Physics* (8th edn). Wiley: Hoboken, NJ, 2005.
76. Hoplzapfel GA. *Nonlinear Solid Mechanics*. Wiley: Chichester, Weinheim, New York, 2000.
77. Nowacki W. *Thermoelasticity* (2nd edn). Pergamon Press: Stanford, 1986.
78. Hughes TJR. *The Finite Element Method*: *Linear Static sand Dynamic Finite Element Analysis*. Prentice-Hall: Englewood Cliffs, NJ, 1987.
79. Jang S, Voth GA. Simple reversible molecular dynamics algorithms for Nosé–Hoover chain dynamics. *Journal of Chemical Physics* 1997; **107**:9514–9526.
80. Jang S, Voth GA. Response to comment on 'Simple reversible molecular dynamics algorithms for Nosé–Hoover chain dynamics' [J. Chem. Phys. 110, 3623 (1999)]. *Journal of Chemical Physics* 1999; **110**:3626–3628.
81. Brańka AC. Nosé–Hoover chain method for nonequilibrium molecular dynamics simulation. *Physical Review E* 2000; **61**:4769–4773.
82. Liu WK, Belytschko T. Mixed-time implicit-explicit finite elements for transient analysis. *Computers and Structures* 1982; **15**:445–450.
83. Torrens IM. *Interatomic Potentials*. Academic Press: New York, London, 1972.
84. Frenkel YI, Kontorova T. The model of dislocation in solid body. *Zh. Eksp. Teor. Fiz.* 1938; **8**:1340 (in Russian).
85. E W, Engquist B, Huang Z. Heterogeneous multiscale method: a general methodology for multiscale modelling. *Physical Review B* 2002; **67**:092101-1-4.
86. Dupuy L, Tadmor EB, Miller RE, Phillips R. Finite-temperature quasicontinuum: molecular dynamics without all the atoms. *Physical Review Letters* 2005; **95**:060202.
87. Sheng N, Li S. A non-equilibrium multiscale simulation of shock wave propagation. *Mechanics Research Communications* 2008; **35**:10–16.
88. Mori H. Statistical-mechanics theory of transport in fluids. *Physical Review* 1958; **112**:1829–1842.
89. Yamada T, Kawasaki K. Nonlinear effects in the shear viscosity of critical mixtures. *Progress in Theoretical Physics* 1967; **38**:1031–1051.
90. Mavrantzas VG, Öttinger HC. Atomistic Monte Carlo simulation of polymer melt elasticity: their nonequilibrium thermodynamics GENERIC formulation in a generalized canonical ensemble. *Macromolecules* 2002; **35**:960–975.
91. Broido DA, Ward A, Mingo N. Lattice thermal conductivity of silicon from empirical interatomic potentials. *Physical Review B* 2005; **72**. Article no. 014308.
92. Cahill DG, Ford WK, Goodson KE, Mahan GD, Majumdar A, Maris HJ, Merlin R, Phillpot SR. Nanoscale thermal transport. *Applied Physics Reviews* 2003; **93**:793–811.
93. Zeng X, Li S. A multiscale cohesive zone model and simulations of fracture. *Computer Methods in Applied Mechanics and Engineering* 2010; **199**:547–556.
94. Li S, Fan H, Sheng N. Multiscale nonequilibrium molecular dynamics simulations: heat transfer and crack propagation. 2009; 1–20. Unpublished.

DOI: 10.1002/nme